Computational Modelling of Drug Delivery to Solid Tumour: Understanding the interplay between chemotherapeutics and biological system for optimised delivery system

Wenbo Zhan[1†], Moath Alamer[2†], Xiao Yun Xu[2*]

1. Department of Mechanical Engineering
2. Department of Chemical Engineering

Imperial College London, South Kensington Campus, London, United Kingdom

* Corresponding author: Professor Xiao Yun Xu, Department of Chemical Engineering, Imperial College London, South Kensington Campus, London, SW7 2AZ, UK. Tel: +442075945588, E-mail: yun.xu@imperial.ac.uk

† The authors made equal contributions to this review.

Abstract

Drug delivery to solid tumour involves multiple physiological, biochemical and biophysical processes taking place across a wide range of length and time scales. The therapeutic efficacy of anticancer drugs is influenced by the complex interplays among the intrinsic properties of tumours, biophysical aspects of drug transport and cellular uptake. Mathematical and computational modelling allows for a well-controlled study on the individual and combined effects of a wide range of parameters on drug transport and therapeutic efficacy, which is not possible or economically viable through experimental means. A wide spectrum of mathematical models has been developed for the simulation of drug transport and delivery in solid tumours, including PK/PD-based compartmental models, microscopic and macroscopic transport models, and molecular dynamics drug loading and release models. These models have been used as a tool to identify the limiting factors and for optimal design of efficient drug delivery systems. This article gives an overview of the currently available computational models for drug transport in solid tumours, together with their applications to novel drug delivery systems, such as nanoparticle-mediated drug delivery and convection-enhanced delivery.

Keywords: drug delivery system, drug transport, solid tumour, mathematical modelling.

1. Introduction

Despite the development of numerous chemotherapeutic drugs with desirable anticancer effects in preclinical trials, their effectiveness in clinical settings remains disappointing. This is partially attributed to the delivery and transport limitations of anticancer drugs in tumour interstitium. In solid tumours there are several barriers posed by the tumour microenvironment. During early tumour growth, cancer cells interact with normal cells and the surrounding tissue to create a microenvironment that promotes malignancy and induces changes leading to the development of complex tissue microarchitecture. Hence, tumour is described not only as a mass of cancer cells but also an abnormal tissue composed of multiple cell types, extracellular matrix (ECM) and its own unique vascular network [1].

Tumour tissue features several distinct biological and biophysical properties. Unlike vasculature in normal tissue which has a well-organised morphological structure, tumour vasculature tends to be poorly organised, with no clear distinction between different vessel types due to erratic changes in diameter, excessive branching and looping. Individual vessels may exhibit cellular abnormalities such as wide inter-endothelial gaps, immature pericyte detachment and lack of basement membrane [2]. This leads to increased fluid leakage into the interstitium, resulting in accumulation of fluid in the interstitial space and elevated interstitial fluid pressure (IFP), which in turn reduces transvascular fluid transport and extravasation of therapeutic molecules [3]. Moreover, tumour extravascular space has higher ECM density than in normal tissue, creating further barrier for interstitial transport. The extracellular space of tumour tissue is also more acidic when compared to normal tissue as some cancer cells can produce energy through glycolysis at a high rate. This highlights the complexity of tumour microenvironment with inter-dependent properties showing spatial and temporal variations.

The transport of cancer therapeutics from their injection site to the intended cellular and intracellular targets involves multiple steps, which span a wide range of length and time scales [4]. Consequently, it is a significant challenge to develop a drug delivery system that is able to overcome the aforementioned transport barriers and take advantage of drug-tumour interplays for improved treatment efficacy. As a cost-effective approach, computational modelling plays an increasingly important role in understanding drug transport in solid tumours for a number of reasons. These include: it can facilitate comprehensive parametric sensitivity analyses to identify the most influential factors; it allows the multiple steps involved in drug delivery to be examined individually and in an integrated manner; and finally, clinically controllable factors, such as drug dose and administration schedule, can be incorporated into the model for *in silico* simulations, which may help reduce the number of laboratory and animal experiments. Once the models are fully validated, they can be used to assist in the design of drug delivery systems for optimal therapeutic responses.

To achieve these objectives, computational models of drug delivery need to provide a detailed description of the series of drug transport steps. A wide spectrum of mathematical models has been developed, which has been the subject of several review articles in the literature [5-7]. In this review, we mainly focus on transport-based models and their applications to different drug delivery systems; these include nanoparticle-mediated drug delivery and implantable drug releasing devices. The article is structured as follows: Section 2 summarises the development of compartmental models based on pharmacokinetics and pharmacodynamics. Transport-based models are described in Sections 3 and 4 for microscopic and macroscopic models, respectively. Section 5 provides examples of the application of a range of computational models in the development of micro/nano drug delivery systems, including thermosensitive liposomes, polymer-based drug carriers and pH-sensitive nanoparticles. Section 6 focuses on implantable drug release devices, where chemotherapeutic wafers and convection- enhanced delivery are covered. Issues related to model validation are discussed in Section 7, and we conclude in Section 8 with a summary of challenges and outlook.

2. Pharmacokinetics/pharmacodynamics-based compartmental models

Pharmacokinetic (PK) models describe the absorption, distribution, metabolism and excretion of substances within a biological system by mass balance equations. In physiologically based pharmacokinetic (PBPK) models, multiple compartments are often required to represent the tissue and organs of interest, with inter-compartment connections through the circulatory system and/or lymphatic system [8]. As such, PBPK models are able to simulate the exchange of drug among compartments and accumulation of drug within a particular organ or tissue. The pharmacological effects of a drug can be quantitatively evaluated by a pharmacodynamics (PD) model which describes the time-course of drug effects on the body [9].

A large number of PBPK and PD models have been proposed for different anticancer drugs, and a few representative models are outlined here. A PK-based model for paclitaxel was developed which accounted for drug binding in the extracellular space (ECS) and intracellular space (ICS), drug elimination in ECS and the effect of tubulin [10], with model validation being performed using *in vitro* experimental data on human breast MCF7 cancer cells. A two-compartment PK model was employed to examine the temporal profile of serum siltuximab concentration, and its effect on C-reactive protein suppression was evaluated by an inhibitory indirect response PD model [11]. Upon validation against experimental data, the authors concluded that this PK/PD model could be used to select drug dosage when designing treatment regimens. By combining intracellular pharmacokinetics of gemcitabine in tumours with a plasma PK model and cell-cycle PD model, an integrated modelling framework was devised [12] which was further validated using *in vivo* patient data. The performance of gefitinib, a EGFR inhibitor, in treating intracerebral tumours was evaluated by a PBPK/PD model, which showed how intra-tumour non-uniformity could lead to variable drug exposure and pharmacological effects within the tumour, and how the model could be utilised to reshape the

treatment regimen with an alternative dosage schedule [13]. Based on *in vivo* data, a PK/PD model for tumour growth inhibitor AZD8055 was built and further refined by using human tumour xenograft model with different drug sensitivities and cell growth rates towards optimising the drug dose and administration route [14].

A typical PBPK/PD model for nanoparticle-mediated drug delivery is schematically described in **Fig. 1**, and the corresponding mathematical equations are summarised in Appendix. In an attempt to predict optimal conditions for maximising the therapeutic efficacy of liposome-mediated delivery of doxorubicin, a PK/PD model was developed [15], where free and liposome encapsulated doxorubicin in the circulatory system was described by a PK model which was linked to the tumour compartment through blood perfusion rate, while the treatment was evaluated in terms of cell number as a function of extracellular drug concentration. The model was validated by animal experiments, but the optimal conditions obtained on experimental animals cannot be extrapolated directly to humans. This modelling framework was integrated with a p53 dynamic network model and cell-cycle model to explore the mechanism of cell apoptosis with liposomal delivery of doxorubicin [16].

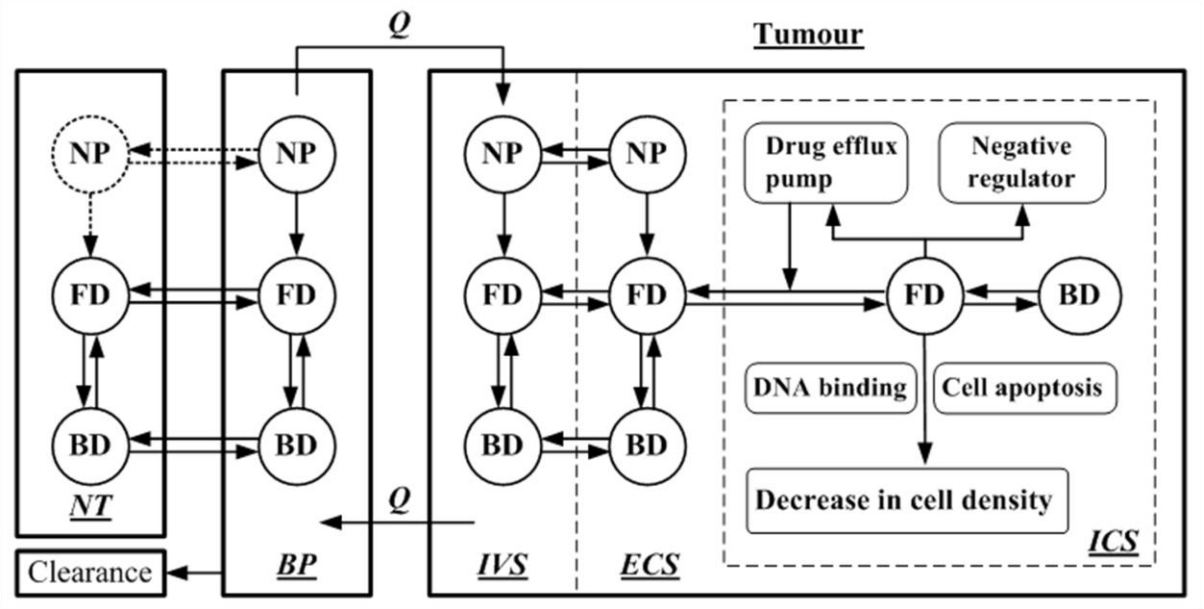

Fig. 1. Different compartments and their connections in a typical PBPK model for nanoparticle-mediated drug delivery to a solid tumour. The biological system is divided into multiple compartments consisting of normal tissue (NT), blood in the circulatory system (BP), tumour intravascular space (IVS), tumour extracellular space (ECS) and intracellular space (ICS). Chemotherapeutics can be present in three forms: nanoparticle encapsulated drug (NP), free drug (FD) and drug bound with proteins (BD). Blood plasma clearance can constantly reduce the concentration of drugs in all three forms in BP. The exchange between BP and IVS compartments is facilitated through blood perfusion rate *Q*. Only free drug can enter ICS for cell killing. NP is usually designed with limited accessibility to NT.

PK/PD-based models can also be modified to examine the impact of drug resistance on therapeutic efficacy. Drug resistance may act by different mechanisms which could be intrinsic or directly

induced by the drug [17]. Acquired or induced drug resistance can arise from enhanced expression of transporters such as P-glycoprotein (P-gp) which is capable of effectively pumping structurally unrelated cytotoxic agents out of cell interior with enough energy supply [18]. The presence of anticancer drugs can further increase the expression level of P-gp during treatment. The role of P-gp mediated efflux in intracellular paclitaxel kinetics was investigated and found to be dominant at the lower end of the clinically observed drug concentration range [19]. The influence of intracellular doxorubicin-mediated P-gp induction on tumour cell killing was examined using a theoretical PK/PD model [20], where the PK model governed the drug extracellular, intracellular and nucleic concentration, as well as the level of P-gp. Tumour cells were assumed to be killed only when the drug nucleic concentration was above a threshold value. The modelling results suggested that drug resistance induced by P-gp overexpression could be partially circumvented by optimising the dosage level [20].

Aimed at improving treatment strategies against cancer, a model that integrated multiple physiological processes was built [21], which included intracellular metabolism, cellular drug effect, cell-cycle progression, nutrient diffusion and pharmacokinetics of drugs. In this model, cell killing by drugs was dependent on cell-cycle phase, while cell-cycle phase transition was controlled by local ATP generation. Concentration profiles of 5-fluorouracil and paclitaxel were predicted by a two- and three-compartment model, respectively.

In experimental studies, the effectiveness of cancer therapeutics is commonly evaluated in terms of tumour volume as a function of time. However, this is not feasible for most mathematical models which simulate a much shorter time window than that required for visible tumour regression. Consequently, in addition to conventional PD models, various empirical correlations have been developed, which usually evaluate cell survival rate (SR) as a function of area under the concentration-time curve (AUC), *e.g.* an exponential relation between SR and extracellular AUC [22], a Hill function [23] or a hybrid model by combining the above two functions in one form with additional parameters [24]. An exponential model accounting for the kinetics of cell killing was also proposed [25], albeit with limited application. Models with SR being related to the peak intracellular concentration or peak DNA-bound cisplatin concentration were found to predict the corresponding cytotoxicity data over a wide range of exposure times up to 121 hours [26]. As the efficacy of a number of drugs is associated with cell-cycle phase, models invoking cell-cycle were further developed with a unique set of parameters for each drug and tumour type [27].

In summary, PBPK models in the form of ordinary differential equations (ODE) are based on the fundamental assumption of homogeneity, with mass conservation serving as the principle for drug exchange among compartments. Additional conceptual compartments can be created and integrated into the model with focuses on particular physiological processes and interplays between chemotherapeutics and various components in a biological system [19, 28]. PD models either treat the

cells as an integrated, single compartment [29] or differentiate the anticancer effect with respect to cell-cycle phases [21]. Coupled PBPK/PD models are capable of predicting drug concentration and cell survivals as a function of time, where model parameters are usually derived from experimental data. Particular attention should be placed on the limitation of extrapolating model parameters derived from animal experiments to humans owing to the physiological differences. Therefore, further model validations are necessary.

3. Microscopic transport models

Microscopic properties of the tumour tissue can have a significant impact on the transport and uptake of cancer therapeutics. These include tumour microvasculature, lymphatics, tumour cells and ECM composition, to name only a few. Mass transport in capillaries and interstitial space is influenced by blood flow, transvascular exchange and interstitial flow, as illustrated in **Fig. 2**. Differing from compartmental models which are described by a set of ODEs, transport-based models use PDEs for explicit descriptions of fluid flow and drug transport in a pre-defined domain of interest, so that they can predict not only temporal variations but also spatial distributions of therapeutic agents. A number of models have been developed focusing on different aspects of the drug transport process.

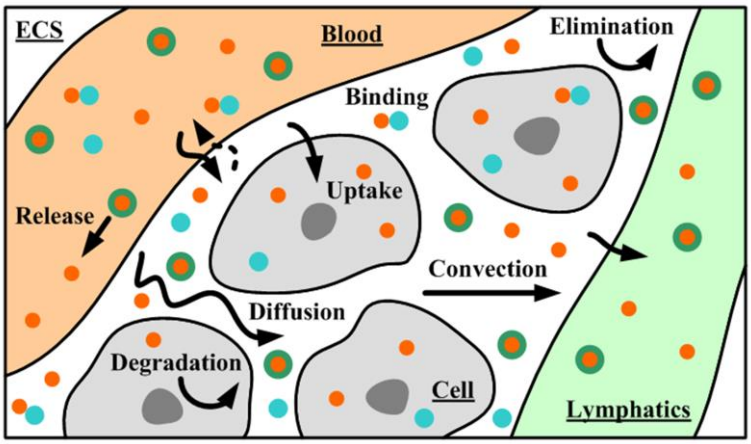

Fig. 2. Representative kinetic and transport processes in nanoparticle-mediated drug delivery to solid tumour. Free drugs can be released from nanoparticles. Both free and encapsulated drugs can transport within blood stream and across the vessel to enter the tissue ECS, where convection, diffusion, cell uptake and elimination take place. The drugs can degrade in cells and be cleared by lymphatics. Drugs can also diffuse back into blood, driven by the concentration gradient across the vessel wall.

3.1. Tumour cord models

Tumour cord models were developed to provide a simplified geometric representation of the *in vivo* tumour microenvironment. In these models a single straight cylindrical blood vessel is surrounded by circumferentially uniformly distributed cells forming a cylindrical unit and the whole tumour is considered an assembly of these tumour cords as illustrated in **Fig. 3**. Within this idealised geometry, nutrient, oxygen and drug concentrations are assumed to decay radially away from the vessel within

the cord. As a result, cellular proliferation decreases when moving towards the periphery of the cord, and at a certain distance from blood vessels cell death occurs forming necrotic regions [30]. This model provided a platform for understanding the ability of drugs to penetrate through layers of cells and reach regions that are distant from the vessel. Previous studies utilising tumour cord geometries coupled PK compartmental models with solute transport principles to describe the spatiotemporal evolution of drug concentrations in a tumour cord. For example, a tumour cord model was used to investigate the penetration of doxorubicin and predict intracellular concentration for different dosage regimens [31], where drug concentration in the capillary was determined by a 3-compartment plasma PK model, while transvascular transport was described by the Staverman-Kedem-Katchalsky equation.

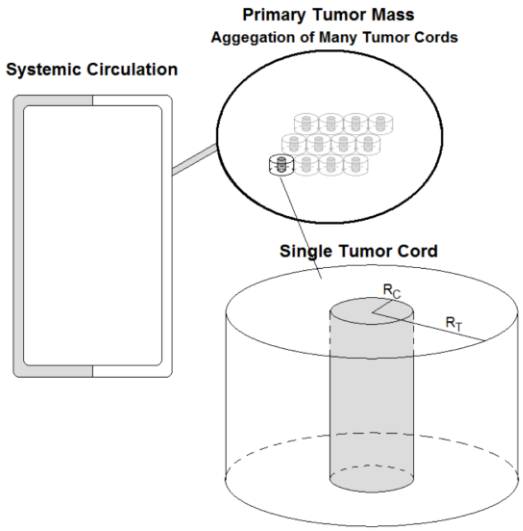

Fig. 3. Tumour cord model where R_T is the radius of a single tumour cord and R_C is the radius of the capillary within the cord. The tumour is assumed to be composed of many individual tumour cords linked to the systemic circulation. Reprint from Ref [31] with open access.

In the interstitial space, therapeutic molecules can be transported by diffusion and convection, although the effect of convection is often neglected except for convection-enhanced delivery. By considering drug transport through diffusion and changes in extracellular and intracellular drug concentrations using the PK model developed by Elkareh and Secomb [32], Eikenberry examined the dependence of therapeutic efficacy on drug dose and showed that rapid bolus was more suitable for low doses whilst continuous infusion for 1 hr would provide optimum therapeutic results for high doses [31]. Additionally, fractioning the dose into several smaller doses provided a slight improvement in therapeutic effect. The effect of tumour microenvironment properties was investigated by varying parameters such as vessel morphology, cell packing density and tumour cord size. Increasing cell density resulted in increased cell killing near the vessel wall but reduced drug penetration depth in the tumour cord, whereas more uniform drug penetration was obtained at low cell density. A different type of tumour cord model was described by Groh *et al*. [6] by exploiting the shell like nature of cells surrounding the vessels, where the geometry of the tumour cord consisted of

concentric spherical shells. Variations along the vessel were incorporated in a more recent study [33] which also included a three-compartment model for extracellular free drug, intracellular free drug and intracellular bound drug. Their model demonstrated that drug penetration could be improved in leakier, wider vessels with high blood velocity. Additionally, their results showed that high diffusion rates led to more uniform drug distribution, whereas slow diffusion caused drug to be concentrated near the vessel.

3.2. Models accounting for tumour vasculature

The tumour cord models described above treat the vasculature in a highly idealised manner, without accounting for the tortuous vascular network. The intricate and complex nature of the tumour microvasculature makes it a significant challenge to model drug transport with explicit description of the vasculature. One of the difficulties is to obtain realistic representations of the vasculature. Previous models of microscopic drug transport used various methods to describe the tumour vasculature. As angiogenesis commonly occurs in tumours as they grow in size, some models have utilised Anderson and Chaplain's tumour-induced angiogenesis model [34] which allows for the simulation of capillary network formation in response to factors secreted by nearby neoplastic cells. The vascular networks generated from this angiogenesis model have been subsequently applied in some fluid flow and drug transport models [34, 35]. Sefidgar *et al*. used the angiogenesis model to study the effect of heterogeneous vascular networks on fluid flow and drug transport [36]. To do this they first modelled a tumour where microvessels were represented as a uniformly distributed source term. Subsequently they modelled a tumour where the microvascular network was explicitly represented for a case with pre-defined vessels and another case with adaptive vessels. Their results showed that the model with an adaptive capillary network had the highest interstitial pressure and that drug distribution was more heterogeneous in cases where blood vessels were explicitly represented, compared to the baseline case with uniformly distributed microvessels.

Whilst Anderson and Chaplain's model provides an estimate of the complex tumour microvascular network, their model does not incorporate all the mechanisms involved in the angiogenesis process. Imaging techniques, on the other hand, offer the possibility of acquiring detailed geometrical information on the vasculature in tumours which can then be incorporated into mathematical models of drug transport. A comprehensive review on imaging techniques for 3-D visualisation of tumour vasculature is available [37], hence in this section we will focus on studies that have combined imaging techniques with tumour drug transport models.

Secomb *et al*. simulated oxygen transport in a rat mammary carcinoma with 3-D networks of microvessels reconstructed from images acquired using an optical sectioning method with a fluorescent confocal microscope [38]. The microvascular network was represented as a set of cylindrical segments whose diameters and coordinates were based on the optical sections. The

drawback of this method, however, was that it was limited to the microscopic scale and did not include the whole tumour vascular network. In fact, obtaining 3-D imaging data on vascular morphology at different spatial scales has been a challenge due to the difficulty of integrating micro and macroscopic images. Stamatelos *et al*. attempted to address this by using a high-resolution *ex-vivo* technique to provide images covering the entire tumour vascular network [39]. In their work, a tumour grown in mice from human breast cancer cells was cast and scanned using μCT, and a bioimage informatics algorithm was developed to track and characterise the vasculature from the acquired images. A 1-D fluid flow model was applied to the reconstructed vascular network to simulate blood flow as shown in **Fig. 4**. Morphological and haemodynamic parameters were calculated for the whole tumour and at different regions of interest.

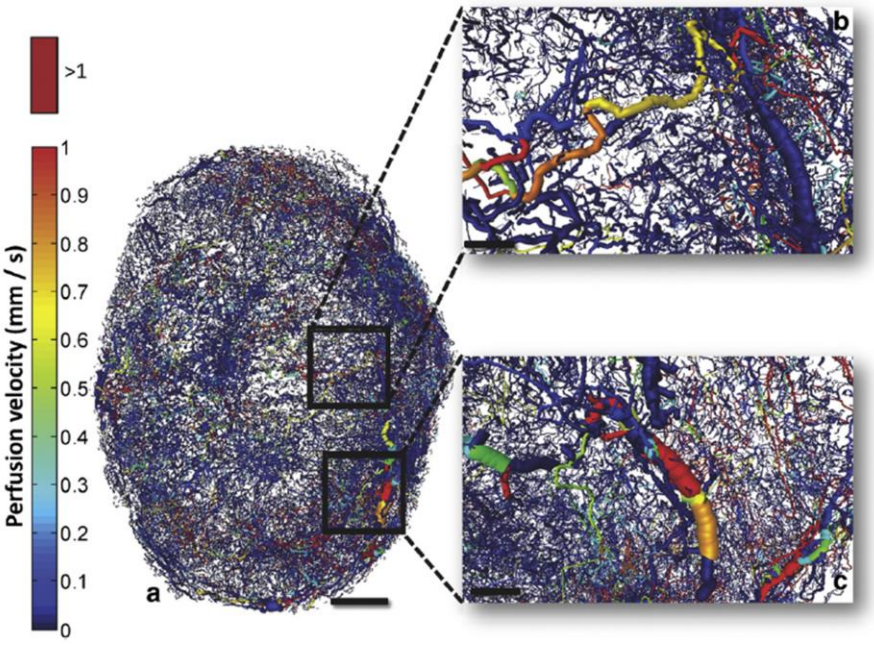

Fig. 4. (a) Reconstructed whole tumour vascular network colour coded by perfusion velocity (mm/s). (b) and (c) are magnified regions within the tumour vascular network. Reprint from Ref [39], with permission from Elsevier.

Fig. 4 highlights another challenge in modelling drug transport in tumours with explicit representation of the vasculature; that is how to solve the drug transport equations in such a complex geometry. A variety of numerical techniques based on finite difference, finite volume or finite element methods have been adopted. Cattaneo and Zunino used a finite element method to build a computational model coupling intravascular flow, transvascular exchange and interstitial flow in a complex tumour microvasculature [40]. To reduce the complexity of the problem and its computational demand, the capillary bed was represented as a network of 1-D channels acting as concentrated sources of flow immersed in the interstitial volume as shown in **Fig. 5**. Their model was used to compare conventional bolus and nanoparticle-mediated delivery of tirapazamine (TPZ). To simulate nanoparticle transport, three stages of the delivery process were accounted for: nanoparticle transport in the capillaries, adhesion of particles to capillary walls and transport of encapsulated drug to the

tumour tissue. The transvascular transport of nanoparticles and their migration in interstitial space were not considered. Comparisons of results from the two drug delivery modalities showed that tissue drug concentration was higher with nanoparticle delivery than conventional delivery at all time-points.

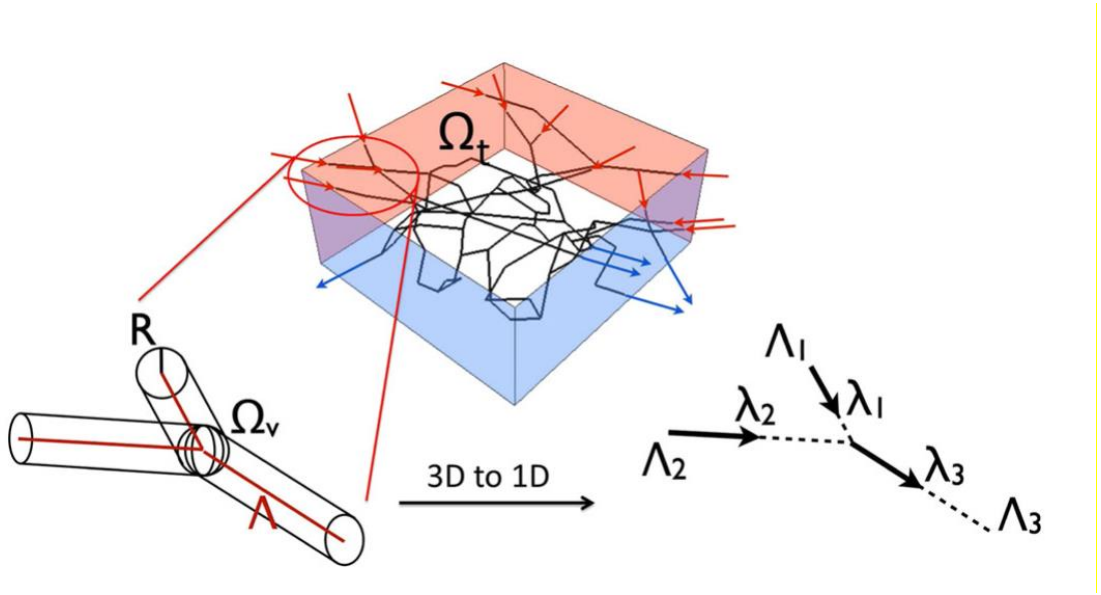

Fig. 5. Tumour tissue with embedded vascular network. Reduction of the capillary vessels from 3D to 1D is visualised. Reprint from Ref [40], with permission from John Wiley and Sons.

Whilst finite difference and finite element methods allow for direct incorporation of features such as time dependence, drug uptake and spatial variations of transport properties, fine meshes are needed to capture the complex geometry of the tumour vascular network which significantly increases the computational demand. Specifically, in regions near the vessel wall drug concentrations can vary greatly over small spatial steps, hence the mesh size and the corresponding time-step size need to be sufficiently small to ensure numerical stability and accuracy. With this in mind Secomb developed a Green's function method whereby each vessel is represented as a distribution of solute sources and the tissue solute concentration field is represented as a superposition of the fields resulting from these sources [41]. This allows for solute tissue concentration to be expressed as a function of vascular structure and morphology, whilst reducing the number of unknowns and computational need. Secomb's method was used to analyse the kinetics of solute washout from heterogeneous vascular networks obtained from rat cremaster muscle. This method was found to provide an efficient means to analyse time-dependent diffusion, convection and reaction in complex geometry systems, showing potential application in understanding the transport characteristics of chemotherapeutic drugs.

3.3. Models accounting for transvascular transport

An essential step for a drug to reach cancer cells is that it must be able to penetrate the vessel wall and reach the tumour tissue. Several studies have focused on transvascular transport mechanism of nanoparticles in tumours. Chauhan *et al*. attempted to investigate the effect of vessel pore size on

nanoparticle penetration in tumours to understand how vascular normalization can improve tumour treatment [42]. They generated a tumour vascular network using a 2D percolation model with varying pore sizes and heterogeneity (**Fig. 6)**. Vascular, transvascular and interstitial flow were coupled and described by Poiseuille's, Starling's, and Darcy's laws, respectively. Discretized vascular points were assigned their own values for hydraulic conductivity, permeability and reflection coefficient to simulate heterogeneous pore size distribution. Their results showed that reducing pore size lowered IFP thus allowing for small nanoparticles to enter through them rapidly. However, this increased the steric and hydrodynamic forces which made penetration of large nanoparticles difficult. As the pore size exceeded 140 nm, drug penetration was restricted due to high IFP and limited convection. Their study concluded that each pore size would have a corresponding ideal nanoparticle size that allows for maximal delivery, and that smaller nanoparticles (<12 nm) would be ideal for improved penetration. This work was further extended to incorporate the effect of surface charge of the nanoparticles and electrostatic interactions with the vessel wall [43], where the vascular network was generated using a tumour induced angiogenesis model [44] and the Poisson Boltzmann equation was adopted to describe electrostatic double layer interactions between the particles and cylindrical pore. It was found that for small pore diameters the electrostatic repulsion affected transvascular transport significantly whereas for larger diameters the effect was negligible. Electrostatic attraction was found to have more impact on transvascular transport as the nanoparticles became larger.

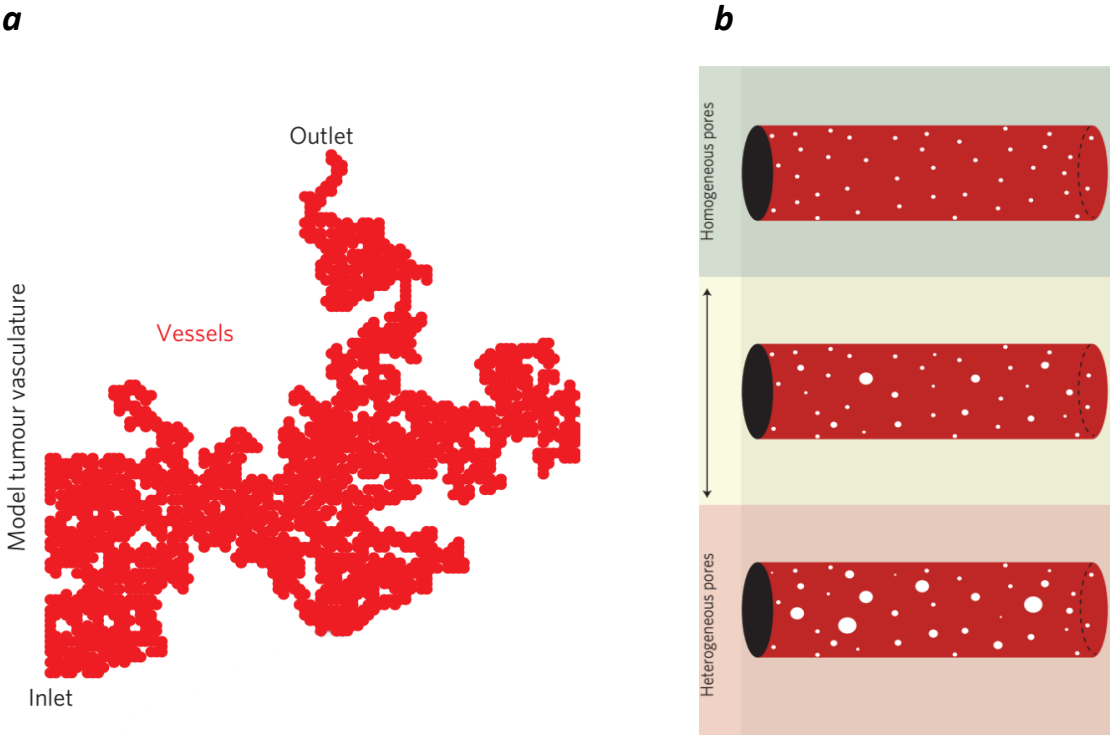

Fig. 6 (a) Tumour vascular network generated through percolation (b) Representation of pore structure. Reprint from Ref [42], with permission from Nature.

Most models treat blood as a Newtonian fluid and neglect the effects of red blood cells (RBCs). In capillaries whose diameters range from 5 μm to 40 μm, the particulate nature of RBCs becomes important and blood viscosity is dependent on shear rate, haematocrit, RBC conformation and aggregation. These properties are expected to have some influence on nanoparticle distribution within blood vessels and their ability to penetrate the vessel wall. An agent-based model was recently developed which accommodated RBCs and their effects on the transport of nanoparticles in a single capillary [45], where fluid flow was governed by the Navier-Stokes equations and Brownian motion was incorporated to describe the random movement of particles [45]. Their findings showed that high haematocrit led to more nanoparticle accumulation within 20 nm distance from the vessel wall. Additionally, for nanoparticles of all sizes, more were able to penetrate the vessel wall in tumour tissue when compared to normal tissue. Particles in the size range of 50-100 nm were still able to achieve efficient delivery in tumour tissue whilst in normal tissue almost no transvascular transport was found to occur.

3.4. Models accounting for heterogeneity of interstitium

Generally, drug transport models that account for heterogeneous vascular networks tend to treat the interstitium as a homogenous porous medium composed of uniformly distributed cancer cells and ECM. However, previous *in vitro* and *in vivo* studies suggested that interstitial transport of drug molecules might be affected by the assembly of ECM and packing density of tumour cells [46, 47]. Rejniak *et al*. developed a computational model of interstitial transport that explicitly took into account the cellular structure of tumour tissue in order to investigate how tumour tissue composition would influence interstitial transport of cancer therapeutic agents [48]. They considered a small 2-D patch of tumour tissue on the order of a few hundred microns where tissue morphology was explicitly defined as shown in **Fig. 7**. Particles undergoing interstitial transport were modelled as discrete particles and their movement was described as a combination of advection and diffusion.

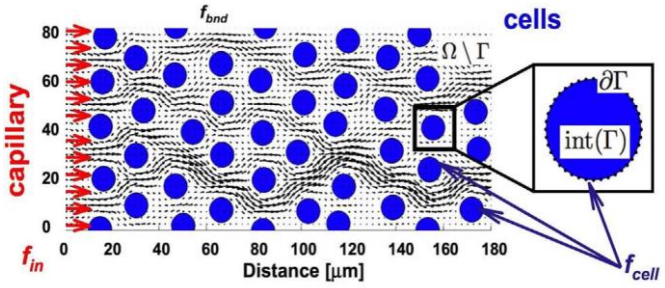

Fig. 7. Representation of interstitial domain containing cancer cells (blue circles) surrounded by interstitial fluid (black arrows). Blood capillary is placed at the boundary on the left (red arrows) where fluid and solutes enter the domain through transvascular exchange. Reprint from Ref [48] **with open access.**

For the advective transport component, fluid flow was calculated through the method of regularized stokeslets, whilst the diffusive component was modelled as Brownian motion. Their interstitial transport model was applied to idealised tissue structures with varying degrees of heterogeneity and cell density. Additionally, histological images of ovarian tumour tissue were digitized and used for computational simulations of interstitial transport. Their study suggested that cellular porosity and density could influence drug penetration in a nonlinear way where sparsely packed tissue showed slower interstitial fluid flow and longer drug penetration time when compared to densely packed tissue. Heterogeneity in tissue morphology resulted in envelopment of tissue zones with low exposure to drugs, suggesting that concentrations in these regions might be insufficient to exert therapeutic effect. Findings obtained from this study highlighted the complex interplay between the heterogeneity of tissue architecture, nanoparticle size and penetration depths achieved. For large, convection-dominated drug particles, tissue regions near the vasculature exhibited low drug exposure, but the particles were able to travel further into the tissue. However, small sized particles with higher diffusivity achieved more uniform tissue penetration near vasculature [48].

In summary, the most advanced microscopic transport models offer the possibility of incorporating the complex tumour microvasculature, transvascular transport and heterogeneous interstitial properties, providing a means to account for tumour-specific microenvironment. Such models can be used to gain more detailed and accurate insight into the transport characteristics of chemotherapeutic drugs at the capillary and cellular level, but extending these models to tissue-scale simulations is a significant computational challenge.

4. Macroscopic transport models

Macroscopic transport models typically treat the tumour as a porous medium where fluid flow and drug transport are described using partial differential equations (PDE). Capillary vessels are usually treated as a distributed or discrete source term, avoiding explicit representation of the tumour vasculature. As such, drug transport at a single capillary level and the spatial relationship between capillary vessels and tumour interstitium are not taken into account. Despite this simplification, macroscopic models can accommodate the effect of realistic tumour size and shape, allowing for prediction of spatial distribution of therapeutic drugs in the entire tumour.

4.1. Model formulation

The mathematical models are based on the mass and momentum conservation equations for interstitial fluid flow, convection-diffusion-reaction equations for the drug (which can be present in free or bound form), and ODEs describing the intracellular drug concentration and pharmacodynamics. The corresponding mass conservation and momentum equations for interstitial fluid flow are:

$$\nabla \cdot \mathbf{v} = F_{BV} - F_{LV}$$
$$\frac{\partial(\rho \mathbf{v})}{\partial t} + \nabla \cdot (\rho \mathbf{v}\mathbf{v}) = -\nabla p_{ECS} + \nabla \cdot \boldsymbol{\tau} + \frac{\mu}{\kappa}\mathbf{v} \tag{1}$$

where ρ and μ are the density and viscosity of interstitial fluid, p_{ECS} and $\mathbf{v}$ are pressure and velocity, respectively, $\boldsymbol{\tau}$ is the stress tensor, and κ is the permeability of tumour/normal tissue, t is time, F_{BV} denotes the interstitial fluid exchange rate between circulatory system and tumour/normal tissue, and F_{LV} is fluid absorption rate due to lymphatic system. Governed by Starling's law, these terms are expressed as:

$$F_{BV} = K_{BV}\frac{S_{BV}}{V_{TU}}\left[p_{IVS} - p_{ECS} - \sigma(\pi_{IVS} - \pi_{ECS})\right]$$
$$F_{LV} = K_{LV}\frac{S_{LV}}{V_{TU}}\left(p_{ECS} - p_{LV}\right) \tag{2}$$

where K is the hydraulic conductivity of vasculature, S/V refers to the vessel surface area per tissue volume, π is the osmotic pressure and σ is the averaged osmotic reflection coefficient for plasma proteins.

Drug transport in the interstitial space can be described by convection-diffusion-reaction equations for each species. For nanoparticle encapsulated drugs and drugs in the free form, these can be written as:

$$\frac{\partial C_{NP,ECS}}{\partial t} = D_{NP,ECS}\nabla^2 C_{NP,ECS} - \nabla \cdot (C_{NP,ECS}\mathbf{v}) + PM(C_{NP,IVS}, C_{NP,ECS}) - k_{rel}C_{NP,ECS} - S_{NP}(C_{NP,ECS})$$
$$\frac{\partial C_{FD,ECS}}{\partial t} = D_{FD,ECS}\nabla^2 C_{FD,ECS} - \nabla \cdot (C_{FD,ECS}\mathbf{v}) + PM(C_{FD,IVS}, C_{FD,ECS}) + k_{rel}C_{NP,ECS} - S_{FD}(C_{FD,ECS}) \tag{3}$$

where D denotes drug diffusivity in the interstitial fluid, and k_{rel} is the drug release rate from its nanoparticle carrier. The term on the left-hand side denotes the variation of drug concentration (C_{ECS}) with time, while the first two terms on the right-hand side represent diffusion and convection, respectively. The third term accounts for drug exchange with blood and lymphatic system, governed by the pore model (PM) in Equation (4), and the last one is the reaction term accounting for all the relevant kinetics, such as binding with protein, physical degradation and cell uptake, *etc*.

$$PM(C_{IVS}, C_{ECS}) = F_{BV}(1-\sigma)C_{IVS} + P_{BV}\frac{S_{BV}}{V_{TU}}(C_{IVS} - C_{ECS})\frac{\mathrm{Pe}_{BV}}{e^{\mathrm{Pe}_{BV}} - 1} - F_{LV}C_{ECS}$$
$$\mathrm{Pe}_{BV} = \frac{F_{BV}(1-\sigma)}{P_{BV}\,S_{BV}/V_{TU}} \tag{4}$$

Representative values for the parameters used in Equations (1-4) are summarised in **Table 1**, while specific model parameters for commonly used anticancer drugs are given in **Table 2.** Discretised forms of the interstitial fluid flow and drug transport equations can be solved numerically subject to

appropriate boundary conditions, providing spatiotemporal profiles of drug extracellular concentrations which are the usual output from a continuum transport-based model. Such a model can be coupled with appropriate PBPK and PD models, in order to predict the therapeutic efficacy of a specific drug or drug delivery system [49]. In the absence of a suitable empirical PD model, the effective extracellular concentration (C_{Eff}), defined as the required drug dose for killing 90% of the tested cells in *in vitro* experiments [50], can also be adopted to evaluate the therapeutic efficacy of a given treatment schedule, with local $C_{ECS} \geq C_{Eff}$ being used as a criteria for effective treatment.

A theoretical framework was established by Baxter and Jain in their series of pioneering work [51-53] to study the transport of immunoglobulin in a spherical solid tumour with homogeneous and isotropic properties. The model was firstly applied to examine the role of IFP and convection in determining drug distribution, and subsequently extended by building in more complexities and realities in the drug delivery process, including heterogeneous perfusion, presence of lymphatic vessels, metabolism and molecular binding. Representative applications include the simulation of nanoparticle-mediated delivery system in a highly perfused tumour [54], and optimisation of drug delivery from intratumorally injected microspheres [55]. Modelling of nanoparticle delivery to multicellular spheroids showed that particle size, binding rate and porosity were key factors for designing nanoparticle-drug carriers [56]. Another study of cationic liposome transport in 3-D tumour spheroids found that the accumulation on cell membrane and in cell interior were more effective than in the interstitial space for this type of chemotherapeutics [57].

Table 1. Parameters for tumour and normal tissues.

Parameter	Definition	Unit	Tumour Tissue	Normal Tissue	Reference
S_{BV}/V_{Tu}	Surface area of blood vessels per unit tissue volume	m^{-1}	20000	7000	[51-53, 58]
K_{BV}	Hydraulic conductivity of the micro-vascular wall	m/Pa·s	2.10×10^{-11}	2.70×10^{-12}	[51-53, 58]
ρ	Density of interstitial fluid	kg/m^3	1000	1000	[58]
μ	Dynamic viscosity of interstitial fluid	kg/m·s	7.8×10^{-4}	7.8×10^{-4}	[58]
κ	Permeability of the interstitial space	m^2	2.19×10^{-17}	$4.52\times10^{-18*}$	[51-53, 58]
p_{IVS}	Vascular fluid pressure	Pa	2080	2080*	[51-53, 58]
π_{IVS}	Osmotic pressure of the plasma	Pa	2666	2666	[58]
π_{EVS}	Osmotic pressure of interstitial fluid	Pa	2000	1333	[51-53, 58]
σ_T	Average osmotic reflection coefficient for plasma proteins		0.82	0.91	[51-53, 58]
$K_{LV}S_{LV}/V_{TU}$	Hydraulic conductivity of the lymphatic wall times surface area of lymphatic vessels per unit volume of tumour tissue	$(Pa\cdot s)^{-1}$	0	4.17×10^{-7}	[51-53, 58]
p_{LV}	Intra-lymphatic pressure	Pa	0	0	[58]
D_c	Cell density	$10^5 cell/m^3$	1×10^{10}	-	[31]
k_{cp}	Cell proliferation rate	s^{-1}	3.0×10^{-6}	-	[59]
k_{cd}	Cell physiologic degradation rate	s^{-1}	3.0×10^{-16}	-	[59]

Table 2. Parameters for chemotherapeutic drugs in solid tumour.

Parameter	Definition	Unit	Fluorouracil		Carmustine		Cisplatin		Methotrexate		Doxorubicin		Paclitaxel	
MW	Molecular weight	g/mol	130.08	[60]	214.05	[61]	300.01	[62]	454.44	[63]	543.52	[64]	853.91	[65]
$P_{ICS\text{-}ECS}$	Partition coefficient between cellular and interstitial phase	-	1.0	[66]	1.0	[66]	1.0	[66]	1.0	[66]	1.0	[66]	1.0	[66]
$P_{CM\text{-}ECS}$	Partition coefficient between membrane and interstitial phase	-	0.1	[67]	10.3	[66]	0.006	[68]	0.01	[67]	0.3	[69]	3162.3	[70]
K_{ECS}, K_{ICS}	Binding constant of bound drugs over free drugs in interstitial and cellular phase	-	0.1	[71]	5.0	[66]	1.0	[72]	0.7	[73]	3.0	[74]	5.1	[10]
D_{ECS}	Diffusion coefficient in tumour ECS	m^2/s	1.2×10^{-9}	[67]	1.5×10^{-9}	[66]	2.5×10^{-10}	[62]	5.3×10^{-10}	[67]	3.4×10^{-10}	[75]	9.0×10^{-10}	[70]
	Diffusion coefficient in normal tissue ECS		4.6×10^{-10}	[76]	3.2×10^{-10}	[76]	2.4×10^{-10}	[76]	1.8×10^{-10}	[76]	1.6×10^{-10}	[76]	1.1×10^{-10}	[76]
P_{BV}	Blood vasculature permeability in tumour	m/s	9.0×10^{-7}	[67]	7.0×10^{-7}	[66]	1.5×10^{-6}	[62]	1.4×10^{-8}	[67]	3.0×10^{-6}	[75]	7.0×10^{-9}	[70]
	Blood vasculature permeability in normal tissue		2.6×10^{-6}	[67]	2.0×10^{-6}	[66]	4.1×10^{-6}	[62]	4.0×10^{-8}	[67]	8.6×10^{-6}	[75]	2.0×10^{-8}	[70]
k_{bd}	Drug elimination to blood capillaries	s^{-1}	1.8×10^{-2}	[67]	1.4×10^{-2}	[66]	2.9×10^{-2}	[62]	2.8×10^{-4}	[67]	6.0×10^{-2}	[75]	1.4×10^{-4}	[70]
k_{md}	Drug elimination due to enzymatic/none-enzymatic reactions	s^{-1}	5.6×10^{-4}	[67]	1.1×10^{-4}	[66]	7.3×10^{-4}	[62]	1.5×10^{-4}	[67]	5.8×10^{-4}	[58]	6.8×10^{-7}	[70]
C_{Sl}	Solubility in water	M	7.69×10^{-3}	[77]	1.87×10^{-2}	[78]	3.33×10^{-3}	[79]	3.74×10^{-4}	[80]	1.84×10^{-3}	[80]	7.03×10^{-6}	[81]
LD_{90}	Drug concentration for killing 90% cells *in vitro*	M	2.00×10^{-6}	[82]	1.49×10^{-5}	[70]	2.00×10^{-5}	[82]	5.94×10^{-5}	[82]	2.39×10^{-6}	[83]	8.90×10^{-7}	[70]

4.2. Models adopting realistic tumour geometry

An attractive feature of continuum transport-based models is their ability to predict spatial distribution of drugs in complex geometry. This enables the model to be coupled with real tumour geometry reconstructed from medical images. Both magnetic resonance (MR) imaging and computed tomography (CT) can provide high resolution anatomical images for 3-D reconstruction of tumour geometry. A 3-D brain tumour model was built from MR images in a comparative study of systemic administration and polymer-based controlled release for IgG delivery into primitive neuroectodermal tumours [84]. The simulation results showed that drug penetration was more dependent on transvascular permeability than drug diffusivity, and that implanting the drug release polymer in the viable tumour zone had improved delivery outcomes. The role of interstitial fluid convection in a MR image-based brain tumour model was examined and it was found that tumour cells near the brain ventricle were less exposed to drugs compared to the distal remnant tumour [85].

The influence of tumour shape and size on drug transport has been investigated. A study using 3-D idealised tumour geometry demonstrated that convection of drugs inside a spheroidal tumour was better than in a spherical model, and that drug delivery was more efficient in tumours with prolate shapes and small volumes [86]. Their finding on the effect of tumour size was supported by a separate study based on five realistic tumour models reconstructed from MR images [87] where tumour volumes varied from 45 mm^3 to 7129 mm^3. By accounting for tumour size-dependent microvasculature density, the authors further demonstrated that transvasular drug transport was more efficient in small tumours, which enhanced drug accumulation in tumour tissues during continuous drug infusion, but could also cause more rapid drug loss after the completion of drug infusion [87].

It is widely recognised that tumour microvasculature is spatially heterogeneous, resulting in non-uniform transvascular flux of drug entering the tumour interstitium. This is especially critical for drug delivered by means of systemic administration. The influence of necrotic core on drug transport has been investigated by several researchers. Using a 2-D model of a liver tumour reconstructed from CT images [58], the simulation results showed that there was a delay in the time course of drug convection in the necrotic core as compared to the viable tumour region. A more elaborate model accounting for the effect of heterogeneous vascular distribution on drug interstitial transport was built by making use of dynamic contrast-enhanced magnetic resonance (DCE-MR) images [88]. Since the extracellular concentration of tracer Gd-DTPA ($C_{GD,ECS}$) can be described by Equation (5), where $C_{GD,ECS}$ is proportional to the relative increase in signal intensity [89], the spatial variation of transvascualr properties (KS/V) can be estimated voxel-by-voxel from DCE-MR images through curve-fitting to the profiles of $C_{Gd,ECS}$ at different time points.

$$\varphi \frac{\partial C_{Gd,ECS}}{\partial t} = F_{BV}(1-\sigma_{Gd})C_{Gd,IVS} + P_{Gd,BV}\frac{S_{BV}}{V_{TU}}\left(C_{Gd,IVS} - C_{Gd,ECS}\right)$$
$$C_{Gd,ECS} \approx \frac{S_g - S_{g0}}{S_{g0}T_{10}r_1} \quad (5)$$

where S_g and $S_{g,0}$ denote the signal with and without the tracer, T_{10} is the relaxation time and r_1 is the reflexivity - both parameters are constant and can be cancelled out during the calculation. Employing a similar approach, the vascular density in a human liver tumour was found to vary between 0.4 to 2.2 folds of its averaged value [75], which caused a non-uniform distribution of drug concentration as shown in **Fig. 8**. In a more recent study [90], liposome-mediated delivery of doxorubicin to a brain tumour was investigated where vasculature heterogeneity was estimated from DCE-MRI with nonuniform porosity being calculated voxel-wise from the images. Simulations showed that stealth liposomes accumulated more effectively and stayed for longer in the tumour when compared to conventional liposomes and doxorubicin in the free form.

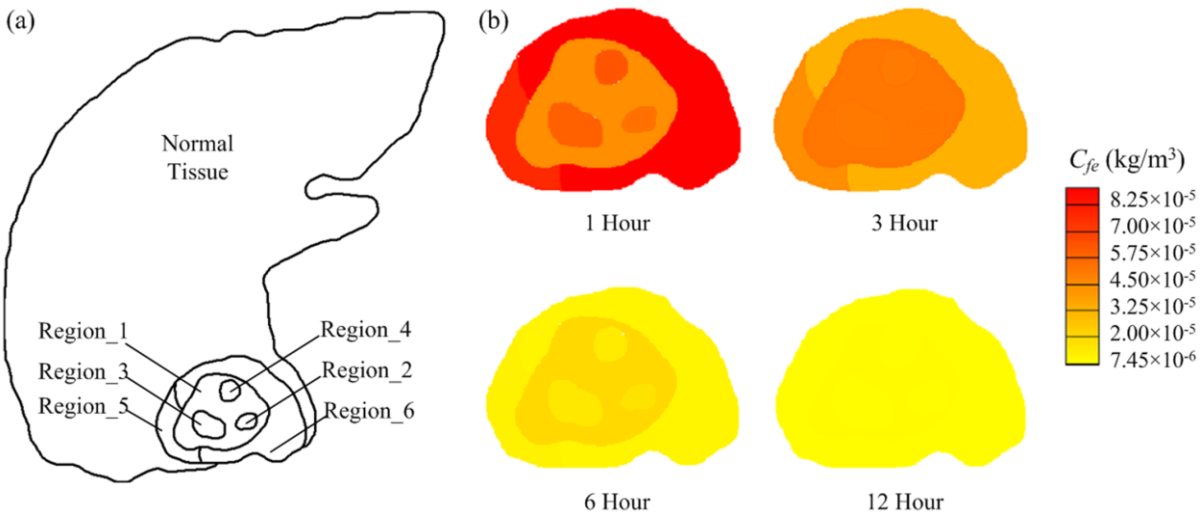

Fig. 8. Image-based geometry reconstruction and simulation. (a) Reconstructed model geometry presenting a liver tumour and its holding tissue, with tumour sub-region 1~6 segmented based on the local image intensity relating to the microvascular density. (b) Free doxorubicin concentration in the extracellular space of the liver tumour at different time points after intravenous administration. Reprint from Ref [75], with permission from IOP Publishing.

Finally, drug transport is subject to directional anisotropy of tumour and normal tissues, especially in the brain. The relationship between MR relaxation times and transport parameters can be described mathematically [91], and the use of diffusion tensor imaging (DTI) for calculation of local anisotropic transport properties of tissue has been validated in animal and human experiments [92]. A computational model for drug transport in anisotropic brain tissue revealed the importance of anisotropic properties in drug distribution in the brain [93].

4.3. Drug transport related dimensionless parameters

Dimensionless numbers are useful in evaluating the relative importance of different factors in determining drug transport [94]. Commonly used dimensionless numbers and their definitions are given in **Table 3**. The ratio of interstitial to vascular resistance (Rt) was introduced to quantify the role of tumour morphology in drug transport [95], and it was found that the optimal volumetric flow rate was proportional to Rt^2 for a spherical tumour. Péclet number and Thiele modulus were analysed in a simulation study [50] comparing the penetration ability of different drugs in brain tumour with wafer implant delivery systems. In this study, experimental data were used to determine model parameters for the tumour and drugs, including microvasculature density, drug degradation and capillary drainage, *etc*. The simulation results demonstrated that the degradation of paclitaxel in a surgically induced cavity was negligible and this drug was free to be transported by convection to reach deep tumour tissue. The dimensionless numbers suggested that 5-fluorouracil showed the most degradation and elimination, presenting the lowest treatment efficacy as compared to the other drugs examined. Based on an evaluation of transvascular Péclet number, the effect of convection was ignored in the simulation of liposome-mediated doxorubicin delivery to brain tumour [96], so that transvascular transport of the drug was assumed to only depend on drug concentration gradient, vessel permeability and vascular density.

Table 3. Dimensionless parameters in drug transport

Symbol	Parameter	Definition	Formula
Rt	-	The ratio of interstitial to vascular resistance to fluid flow	$\mathrm{Rt} = R_{TU}\sqrt{\frac{K_{BV}S_{BV} + K_{LV}S_{LV}}{\kappa V_{TU}}}$
$\mathrm{Pe}_{\mathrm{ECS}}$	Péclet number (for transport in ECS)	The relative importance of drug convection to diffusion	$\mathrm{Pe}_{\mathrm{ECS}} = \frac{v_{ECS}}{D_{ECS}}R_{TU}$
$\mathrm{Pe}_{\mathrm{BV}}$	Péclet number (for transvascular transport)	The relative importance of drug convection to diffusion	$\mathrm{Pe}_{\mathrm{BV}} = \frac{F_{BV}(1-\sigma)}{P_{BV}S_{BV}/V_{TU}}$
Th	Thiele modulus	The relative importance of drug elimination to diffusion	$\mathrm{Th} = R_{TU}\sqrt{k_{elim}/D_{ECS}}$
Ka	Karlovitz number	The relative importance of convective transport to drug elimination	$\mathrm{Ka} = \frac{v_{ECS}}{R_{TU}k_{elim}}$
IC	-	The relative importance of convection	$\mathrm{IC} = \frac{v_{ECS}}{\sqrt{D_{ECS}k_{elim}}}$
He	Heterogeneity	The degree of non-uniformity of drug spatial distribution	$\mathrm{He} = \frac{\Sigma\lvert C_{ECS,i} - C_{ECS,avg}\rvert V_i}{C_{ECS,avg}V_{TU}}$

***** k_{elim} refers to drug elimination rate, R_{TU} is the equivalent radius of tumour/normal tissue with the same volume.

5. Micro- and Nano-delivery systems

For a drug delivery system to be effective it should satisfy a few key requirements. First, it must be able to retain its drug contents and evade the body's defence system in order to reach the tumour site. Given the toxicity of many anti-cancer drugs, delivery systems must be able to target the tumour site to maximise drug accumulation in the tumour interior and minimise drug concentration in systemic plasma and normal tissue. Finally, once in the tumour tissue it must be able to release the drug to achieve the desired therapeutic effects. Many nano-scale anti-cancer drug delivery systems have been developed in recent years that have been engineered from various materials such as polymers, lipids and graphene [97-100]. From these nanomaterials, different shapes and morphologies can be designed including nanoparticles, liposomes, micelles, vesicles, microspheres and micro/nanofibers. These drug delivery systems can be made to possess desirable properties such as optimal size range, longevity *in vivo* and stability, to allow for drugs to be transported into the tumour site where they can be released at a sustained rate through passive mechanisms (enhanced permeability retention effect) or active mechanisms in response to stimuli (pH, temperature, ionic strength *etc*.) [101, 102]. At the same time, considerable efforts have also been made in using mathematical and computational modelling techniques to help understand, develop and optimise micro- and nano-scale tumour-targeted drug delivery systems.

5.1. Modelling of thermo-sensitive liposome mediated drug delivery system

Thermo-sensitive liposome (TSL) mediated drug delivery is a promising alternative to conventional chemotherapy. For well-designed TSLs that are stable at physiological temperature, the encapsulated drugs can only be released when the local temperature is raised above the phase transition temperature of the liposome membrane.

PBPK-based compartmental models are commonly used to compare the predicted treatment efficacy of TSL-mediated delivery with direct infusion of doxorubicin. When using peak intracellular concentration and plasma AUC to evaluate treatment efficacy, a comparative study showed that TSL-mediated delivery was superior only if blood in the sonication zone was not significantly heated [32]. Another study comparing TSL delivery with stealth liposome and conventional chemotherapy of doxorubicin [103] showed that higher local drug concentration in the tumour and lower systemic drug exposure could be achieved with TSL. While stealth liposomes were able to result in higher concentration in the tumour than conventional chemotherapy, their bioavailability was relatively low. This model also predicted different optimal release rates for maximum intracellular concentrations for stealth liposomes and TSL with extravascular or intravascular release [103]. A parametric sensitivity study for TSL mediated doxorubicin delivery was carried out to evaluate the influence of model parameters on peak intracellular concentration [104], and the results revealed that drug release rate was the most influential parameter among blood perfusion, plasma clearance, transvascular and

transmembrane properties. It was also found that drug release rate and heating duration had a saturable effect on peak intracellular concentration, suggesting that these two parameters could be optimised for a given TSL delivery system.

Transport-based continuum models have also been applied to liposomal delivery of doxorubicin in solid tumour. The spatial distribution of encapsulated and free doxorubicin in a 2-D idealised model consisting of 3 regions (a central necrotic core, a peripheral tumour region and its surrounding normal tissue) was analysed using a macroscopic transport model accounting for diffusion and reaction (ignoring the effect of convection) [105]. The computational results showed that enhanced drug delivery upon hyperthermia was limited to the peripheral tumour region, and drug could hardly reach tumour cells in the central region. Another study on the spatial distribution of doxorubicin in a 2-D idealised tumour employed the full transport equation including the convective effect, and their results revealed the potential advantage of TSL mediated delivery in reducing drug accumulation in normal tissue while achieving a much higher peak intracellular drug concentration in the targeted tumour compared to direct infusion of doxorubicin [106].

High intensity focused ultrasound (HIFU) has been adopted as the preferred heating method to achieve local hyperthermia required to trigger drug release from TSL. Attempts have been made to integrate a heat transfer model based on the bioheat equation and a macroscopic transport model, in order to simulate spatiotemporal variations of tissue temperature as well as the consequent drug release and transport. Applying a coupled heat transfer and drug delivery model implemented in finite element software COMSOL to a 2-D axisymmetric geometry, TSL drug delivery triggered by HIFU heating was simulated, and the results suggested a direct association between drug uptake by tumour cells and the duration of hyperthermia, with the maximum drug accumulation being achieved after 2-hour HIFU heating [107]. This model incorporated temperature dependence of key transport properties, including vasculature permeability, diffusivity, transmembrane rate and blood perfusion rate. The bioheat equation included convection associated with interstitial fluid flow, conduction, convective effect due to blood perfusion and HIFU heating. A complete list of heat transfer equations and model parameters can be found in [108].

For tissue heating with HIFU, it is desirable to keep the tissue temperature within a narrow hyperthermia range which should not exceed 43^{o}C to avoid causing irreversible tissue damage [109, 110]. A feedback control system based on a proportional-integral-derivative plus step function was developed for this purpose [111], which showed that there was an optimal controller gain for minimizing the peak temperature overshoot. Further simulations and experiments demonstrated the application of an auto-regressive moving average approach in reducing the effects of temperature fluctuation. The feasibility of closed-loop feedback temperature control in TSL-mediated delivery of doxorubicin under HIFU heating was evaluated [112], in which spatial HIFU heating was controlled

by eight feedback controllers along the ultrasound scanned trajectory according to the proportional-integral (PI) control Equation (6).

$$k_{con}(t) = k_P\left[T_{target} - T_{mor}(t)\right] + k_I \sum\left[T_{target} - T_{mor}(t)\right] \quad (6)$$

where k_{con} is a time-dependent adjustment factor needed for projecting the acoustic power onto the focused region. T_{target} is the target temperature for HIFU heating and T_{mor} refers to the monitored temperature. k_P and k_I are controller parameters.

Attempts have also been made to integrate the acoustic model for HIFU [113] in a numerical platform for TSL-HIFU delivery system. Simulations of acoustic steaming and convective cooling in vasculature during HIFU heating showed a good agreement with experimental measurements [114], although non-linear wave propagation was neglected in this study. The non-linear Westervelt equation was adopted to model the incident finite-amplitude wave propagation of HIFU in heating of liver tumours [115, 116], with a particular focus on the impact of blood convective cooling on the temperature field. The energy equation in this model involved two heat sinks to account for forced blood convective cooling and tissue perfusion, respectively. 3-D modelling results showed that both convective cooling and acoustic streaming could considerably change the temperature field in large blood vessels and the surrounding thermal lesion, leading to blood flow and mass flux redistribution.

One limitation of the acoustic models described above was that they were developed for ultrasound traducers with a single element. Taking advantages of ultrasound phase differences, multi-element transducers have been used in clinical settings to simultaneously generate multiple focus regions with the aim of achieving a homogenous temperature distribution and fast temperature elevation. Fast nearfield method [117, 118] and angular spectrum approach [119-121] have been developed to predict the acoustic pressure field, and have been implemented in a MATLAB code, FOCUS [117, 119, 122]. The calculated acoustic pressure (p_{US}) can be imported into a bioheat transfer model to predict spatiotemporal variations of temperature in solid tumours and surrounding normal tissue. It is hoped the bioheat transfer results obtained from simulations of HIFU with multi-focus regions will be coupled with a continuum-based transport model in the near future.

5.2. Polymer-based drug nanoparticles

Polymer-based drug carriers have been increasingly popular as vehicles for anti-cancer drugs due to their specific tumour targeting ability and reduced toxicity. Most anti-cancer drugs such as doxorubicin and paclitaxel are hydrophobic which leads to low bioavailability and poor delivery. Amphiphilic copolymers composed of hydrophilic and hydrophobic blocks can self-assemble and encapsulate these drugs to allow for increased circulation time and accumulation within tumour tissues [123]. Different morphologies can be formed from the copolymer self-assembly depending on the type of polymer used, its concentration and any added functional groups. The morphology of the

assembled nanoparticle has a strong influence on drug loading, stability and release from the nanoparticle. Several review articles have extensively covered the experimental work on polymer-based nanoparticles and recent advances in their use for cancer therapy [124-126]. Given the plethora of material that can be tested and the limited amount of drug available for multiple experimental runs, computational methods employing molecular dynamics (MD) have emerged as a more economic and feasible way to gain insight into the microscopic mechanisms of nanoparticle assembly, drug encapsulation and release. Furthermore, the processes of drug loading and release occur on the order of several microseconds and on the length scales of several ångströms making it difficult for direct experimental measurements. Therefore, MD simulations have been used to compliment experiments and provide a template for the design of polymer and drug configurations with desirable properties.

The underlying methods of MD involve the study of microscopic interactions between atoms and molecules by solving second order differential equations based on Newton's second law:

$$\mathbf{f}_i = m_i \mathbf{a}_i \qquad \mathbf{f}_i = -\frac{dV(\mathbf{r}(\mathrm{t}))}{d\mathbf{r}_i(t)} \tag{6}$$

where **f** is the net force acting on atom *i* at time t. *m*, **a** and **r** are the mass, acceleration and position coordinates of atom *i* at time t. The interaction between each particle is described by the potential energy *V* which is a combination of bonded and non-bonded interactions. Bonded potentials are a function of bond-stretching, angle bending and torsional rotation between the interacting sites, whilst non-bonded potentials are represented by Van der Waals and electrostatic interactions. Parameter and equation sets obtained empirically, define these interactions for atoms or particles and are collectively known as a force field (FF). Data from MD simulations can be used to provide solutions for optimized geometry, surface chemistry or other properties of drug nano-carriers [127]. A number of molecular modelling approaches have been developed to study systems at different spatial and time scales [128]. For mesoscopic systems where the nanoparticles are as large as 200 nm, Coarse-Grained (CG) or Dissipative Particle Dynamics (DPD) methods are generally used as they are relatively fast and allow for simulations to run for much longer time compared to atomistic simulations [129] [130].

Several authors have reviewed the use of computational methods to study polymer-based drug delivery systems for different drugs [131, 132]. In this section we will give some examples of MD modelling studies for anti-cancer DDS. Costache *et al*. combined all atom MD simulations with docking calculations to model drug interactions with triblock ABA copolymer where the hydrophilic A blocks were made up of PEG and the hydrophobic B blocks were tyrosine derived polyarylates [133]. They modelled the interactions of three drugs, which included paclitaxel with the copolymer. They showed that drug loading was not directly linked to its hydrophobicity and that structural features of the polymer could affect drug loading by influencing hydrogen bonding, π-π stacking, or hydrophobic interactions. Paclitaxel was found to have fewer interactions and lower binding affinity

when compared to other drugs investigated which could be attributed to its larger size and low hydrogen bonding. Guo *et al*. used DPD simulations in several studies of drug carriers with hydrophobic blocks made from poly(lactide)(PLA) polymers [134]. In one of the studies, they mapped a phase diagram of paclitaxel loaded poly(ethylene oxide)-b-poly(L-lactide)(PEO11-b-PLLA9) copolymers [135], showing that the volume fraction of the drug and polymer in the solvent had a strong influence on the size of microspheres, rod, bicontinuous and lamellar structures. Guo *et al*. further expanded their work to study the microstructures of paclitaxel loaded PEO-b-PLA stereocomplexes including poly(L-lactide) (PLLA) and poly(D-lactide) (PDLA) [136]. Initially, they simulated pure paclitaxel in water at different concentrations to find that at low concentrations, paclitaxel molecules formed ribbon like structures whilst at high concentrations, they formed fibre structures. When simulated in the presence of PEO-b-PLA, paclitaxel acted as a template where polymer molecules assembled around the drug forming microfibres that led to the encapsulation of the drug molecules in the PLA core with PEO forming the shell. This agreed with their previous experimental observations [137]. The effect of PLA chirality on drug distribution within the core was investigated by simulating paclitaxel with PEG-b-PLLA, PEG-b-PDLA and their stereocomplexes. Whilst in the PEG-b-PLLA and PEG-b-PDLA systems, paclitaxel was distributed homogenously, for the PLA stereocomplexes there was a thicker PLA core shell causing paclitaxel molecules to be more concentrated in the core as seen in **Fig. 9**. This can enhance the stability of the nanoparticle and slow the release rate of paclitaxel. The influence of PLA length was also studied showing that with increasing PLA length the crystalline structure of paclitaxel was weakened and eventually destroyed which was validated experimentally by X-ray diffraction studies. This can be used to prevent paclitaxel aggregation and enhance distribution at the molecular level.

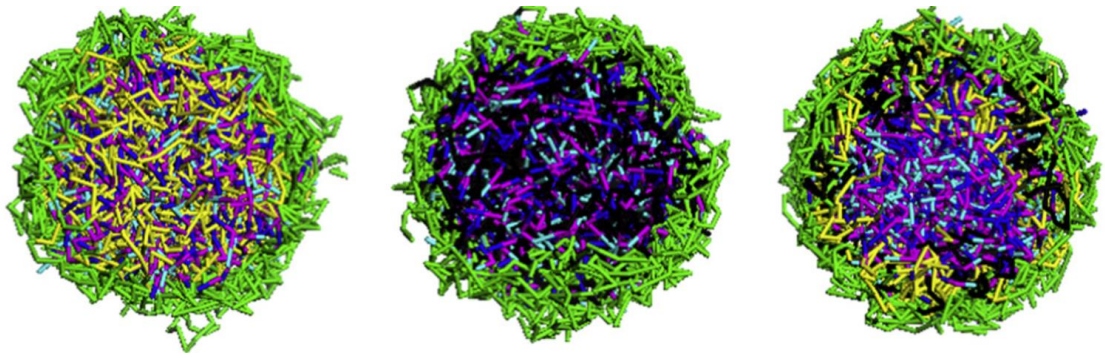

Fig. 9. Cross-sectional views of fibre like structures formed of Paclitaxel with PEO-b-PDLA (left), PEO-b-PLLA (centre) and Stereocomplexes (right). PEO, PDLA and PLLA are represented by green, yellow and black colours respectively. Paclitaxel molecules are represented by blue, purple and light blue. Reprint from Ref [136], with permission from Elsevier.

Polyamides are another class of polymers that can be used to make up the hydrophobic blocks of copolymers for anti-cancer drug delivery. Recently, a linear-dendritic block copolymer named

telodendrimer was synthesised using PEG connected to core forming Cholic acid (CA) through dendritic poly lysine (LYS) [138]. Jiang *et al*. studied the interactions between telodendrimer (PEG-b-CA) blocks and paclitaxel using a multiscale approach, which utilised the MARTINI CG mapping scheme whereby each particle's chemical representation is preserved whilst reducing the number of particles in the system [139]. In their simulations the telodendrimers could aggregate into micelles over a number of microseconds after which a reverse mapping algorithm was applied to obtain atomistic level details. Simulations were performed for a number of systems with varying PEG length and CA amphiphilicity to understand their effects on the self-assembly process and drug loading capacity of paclitaxel. Their results showed that in the absence of paclitaxel, self-assembly was highly sensitive to the number of CA groups and the length PEG chains. When paclitaxel was incorporated into the simulation, it was found to form oil droplets that interacted with the telodendrimers to form spherical micelles. Increasing the percentage of drug loading reduced the encapsulation efficiency whilst increasing micelle size. As the amount of drug in the core increased the micelles became more unstable as the telodendrimers were unable to shield the paclitaxel. Their work further showed that hydrophilic cholic acid telodendrimers did not form a stable micelle core whilst hydrophobic cholic acid interacted favourably with the hydrophobic paclitaxel molecules to form more compact cores. Their computational results were in good agreement with experimentally determined micelle size distributions for different telodendrimers.

Hyperbranched polyesters are polymers that can be considered as a cost-effective alternative to dendrimers. They can encapsulate drugs within their branches, but have poor water solubility; the latter can be improved through PEGylation. Karatasos used all atom MD simulations to examine the assembly of doxorubicin and its interaction with PEGylated hyperbranched polyesters at physiological pH and temperatures [140]. Neutral and protonated forms of doxorubicin were simulated in a polymer free system and in two variants of the polymeric compound with different hydrophilic PEG arm lengths. In all cases doxorubicin was found to self-assemble into clusters of stacked molecules. However, the orientation of drug molecules, the distribution of aggregates and bonding formed between drug and polymer molecules varied depending on the structural properties of the polymer. In comparison to the polymer free system, doxorubicin molecules aggregated more effectively in the presence of the polymer, providing higher local concentrations of the drug. Comparisons between charged and neutral doxorubicin systems showed differences in their structural organisation, with the charged doxorubicin system having stronger hydrogen bonding was stronger, which could be utilised to enhance drug loading and improve therapeutic action. Additionally, the motion of doxorubicin molecules was found to be more constrained in the presence of the polymer, especially as the PEG arm length was increased, leading to the formation of more ordered structures with strong bonding to the polymer. This improved stability helped to facilitate more efficient drug transport to the tumour

with effective release profiles. These findings were consistent with an experimental study on the therapeutic action of the same polymer-drug complex [141].

Chitosan is a polymer that has been used as the hydrophilic shell block in the preparation of nanoparticles as it possesses some desirable properties of drug carriers. However, its application has been limited by its high molecular weight, high viscosity, and poor solubility. This issue was highlighted in a computational study by Subashini *et al.* who modelled the uptake of doxorubicin by six different polymers and Chitosan was found to have the poorest drug uptake [142]. In their work the interaction energies were calculated for each polymer and correlated to drug uptake efficiencies determined experimentally. Chitosan can be modified by depolymerisation to produce Chitosan oligosaccharide (COS) which has enhanced solubility and provides an alternative for use in nanoparticles as it has shown good bioavailability, biocompatibility and low toxicity. Using an all atom MD method Wang *et al.* investigated the encapsulation of paclitaxel in salicylic acid (SA) derived COS nanoparticles [143], and the COS/SA particles were found to spontaneously encapsulate paclitaxel in water environments and were driven mainly by Van der Waals and hydrophobic forces. The COS and SA particles formed with a hydrophilic shell and a hydrophobic core which could potentially enhance the solubility of paclitaxel and hydrophobic anti-cancer drugs. Three different drug loading mechanisms were studied to obtain the optimal theoretical drug/polymer ratio which was found to be 10% (w/w). Shan *et al*. performed MD studies on COS systems with doxorubicin [144]. In their work different acids were used to modify the hydrophobicity of COS. In the drug loading process, π-π interactions were found to contribute greatly in COS/SA and COS/IMN systems. When observing the phenomenon of doxorubicin encapsulation by a single COS chain, it was found to depend mainly on the high binding strength and the development of a sandwiched configuration where the hydrophobic part of the drug carrier was buried so that hydrophobic interactions with the drug were maximised. They investigated the solvent structure around doxorubicin and COS to understand how it may influence the doxorubicin binding process. It was found that for grafted COS systems, the surrounding water structure had an impact on the way doxorubicin and the drug carrier bound to each other. Hydrogen bonds formed between doxorubicin and the COS systems are known to have a major influence on drug loading capacity and hence they were analysed with results showing that electrostatic interactions between the drug and its carrier has a linear relationship with the number of hydrogen bonds formed. The predicted interaction strengths between doxorubicin and hydrophobically modified COS were in good agreement with the corresponding experimental data. From their computational model, Shan *et al.* suggested that blocks with strong hydrophobicity and aromaticity might form stable carriers with high loading rates of doxorubicin [144].

5.3. pH-sensitive nanoparticle delivery systems

The extracellular space of most tumours tends to be acidic with pH ranging from 5.8 to 7.6 which is lower than the average normal tissue pH of 7.5 [145]. This difference has been exploited to develop

pH-sensitive nanomaterials that allow for targeting of the tumour tissue and thus improve drug accumulation and uptake [146, 147]. Functional groups can be added to polymers which become protonated at low pH causing them to become non-ionic and hydrophobic. The increase in hydrophobicity leads to micellar aggregation and destabilisation of the polymer. Hence, these nanoparticles have the ability to encapsulate and store the drug at physiological pH values and then as they enter the tumour extravascular space, the exposure to lower pH values causes the nanoparticles to undergo structural changes that allow for rapid drug release [148]. MD-based studies have been performed on these nanocarriers to understand the mechanisms of drug loading and release in response to pH conditions. Guo *et al*. recently developed pH-sensitive micelles assembled from Cholesterol-Conjugated Peptides $His_{10}Arg_{10}$ (HR20-Chol) [149]. DPD simulations and experiments were performed to study the effect of pH on the microstructure of doxorubicin-loaded micelles by characterising the critical micelle concentration (CMC) and the effect of pH on drug release [150]. With regards to micelle formation, their simulations showed that the CMC was higher at pH< 6.0 than that at pH > 6.0. Analysis of drug loading showed that higher concentrations of doxorubicin could be loaded into the micelles at higher pH values. This highlights the role of pH levels in micelle formation and drug loading where higher pH values facilitate the formation of micelles that can encapsulate higher concentrations of drugs. Simulations investigating the effect of pH on the structure of micelles showed that as the pH value fell below 6.0, the pH-sensitive histidine layers transformed from a dense to swollen state which created channels in the micelles that could promote the diffusion and release of doxorubicin as seen in **Fig. 10**. These simulation results were found to be qualitatively consistent with their experimental data.

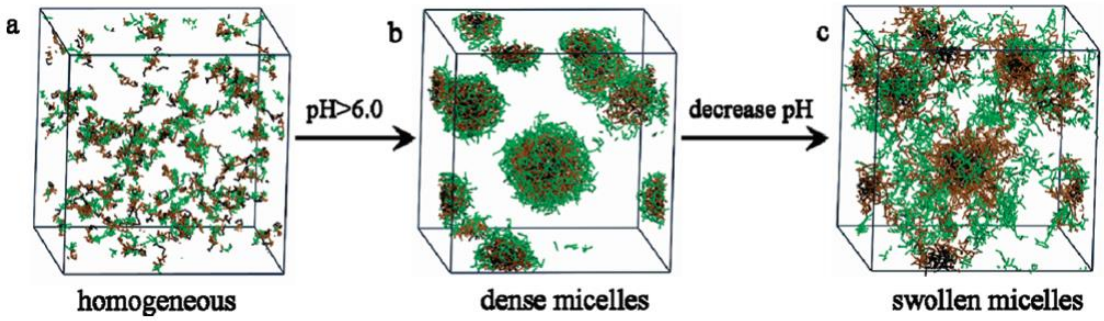

Fig. 10. HR20-Chol system where green, brown, and black lines represent arginine, histidine, and cholesterol, respectively. (a) Initial homogeneous state pH>6.0 (b) Self-assembly of micelles at pH>6.0 (c) As pH is decreased micelles undergo structural transformation which can promote drug release. Reprint from Ref [150], with permission from ACS Publications.

Nie *et al*. applied a similar DPD method to investigate the micelles formed from pH-sensitive four arm star triblock poly(ε-caprolactone)-b-poly(2-(diethylamino)ethyl methacrylate)-b-poly(poly-(ethylene glycol) methyl ether methacrylate) 4AS-PCL-b-PDEAEMA-b-PPEGMA loaded with doxorubicin [151]. This pH-sensitive micelle was synthesised previously in their group and

experimentally studied to show the pH-dependent release behaviour of doxorubicin [152, 153] From their DPD simulations they showed that increasing micelle size led to an increase in doxorubicin concentration, however, gaps began to appear in the PEG layer which caused the micelle to become unstable. Changes in the system pH resulted in different morphologies of the micelle being formed as the pH sensitive arm PDEAEMA became protonated and its solubility changed. Lowering of the pH to 5 resulted in more cracks and gaps being formed in the PEG layer, allowing the doxorubicin to release from the micelle. A similar DPD method was used to investigate the relationship between the structures of pH-sensitive copolymers $A_lB_mC_n$ and the drug release behaviour of the micelles with different drug distributions [154]. When the pH-sensitive copolymer was transferred to an acidic environment, observation of the structural transformation of the micelle showed the pH sensitive blocks extended and the micelle transitioned to a firework-like three layered structure with many channels appearing that can facilitate drug release from the micelles. Analysis of the effect of drug distribution showed that drug released easier and at a faster rate when it was loaded into the pH sensitive layer than in the core.

In the DPD methods employed in the above works, the Flory-Huggins parameters used to determine the maximum repulsion between beads were estimated from solubility parameters. This method works well on non-polar systems without spatial interactions, but it is not reliable for polar systems. This limitation could be overcome by performing atomistic MD simulations to estimate the Flory-Huggins parameters. Luo *et al.* implemented this method where they used fully integrated MD and DPD simulations to investigate the loading and release of anticancer drug camptothecin (CPT) in pH-sensitive amphiphilic copolymers composed of hydrophobic poly(β-amino ester) PAE and hydrophilic PEG [155]. It was found that at low concentrations the copolymers formed small spherical micelles and as concentration increased, disk like micelles developed and finally vesicles began to form. During loading, the process was governed by the adsorption-growth-micellization mechanism where CPT was initially absorbed onto the small clusters formed by polymer chains and as the clusters grew, CPT was loaded into large micelles. Loading of high concentrations of CPT caused the micelles to undergo structural transition to vesicles. When the environment pH was lowered, PAE underwent protonation to become PAEH, causing the micelles or vesicles to swell rapidly and then demicellise to release CPT.

Recent interest has been developed in using zwitterionic materials due to their low-fouling property as PEG polymers can be susceptible to fouling in biological media due to oxidation damage [155]. Min *et al*. performed DPD simulations to study pH-sensitive zwitterionic tri block copolymers poly (ε -caprolactone) −b- poly(diethylaminoethyl methacrylate) −b- poly(sulfobetaine methacrylate) (PCL-PDEA-PSBMA) loaded with doxorubicin [156]. The focus of their work was to investigate the formation of drug loaded micelles and the release mechanisms of doxorubicin at neutral and acidic pH levels and make comparisons with PEGylated polymers (PEGMA). The Flory-Huggins parameters

were determined by combining solubility parameters and all atom molecular dynamics. The copolymers were found to be able to self-assemble into core shell corona micelles, but the corona structures were different between the copolymers. Whilst the shell layer sizes formed in PCL-PDEA-PSBMA micelles were homogenous, in the PEGMA systems they tended to be heterogeneous. When the concentration of the copolymers was increased, the microstructures formed by the zwitterionic polymer and doxorubicin remained as spherical micelles, whilst for the PEGMA the structure transitioned from spherical to cylindrical and finally to lamellar shaped micelles. When analysing the drug release mechanism, as the pH was reduced from 7.4 to 5, the micelles began to swell and drug release occurred instantaneously following demicellisation as seen in **Fig. 11**. The zwitterionic tri block copolymer system was studied experimentally by Zhai *et al.* [157].

Carbon based materials such as graphene and graphene oxide (GO) have recently attracted focus for drug delivery applications [158]. GOs are two-dimensional one atom thick nanosheets with a large surface area that allows for higher drug loading capacities. Drug adsorption on the GO surface is influenced in large part by the electrostatic interactions and hydrogen bonding and as result the environmental pH can have exploited to control drug release and loading. Mahdavi *et al*. used MD simulations to investigate the effect of pH on diffusion, loading and release of doxorubicin in graphene (PG) and graphene oxide (GO) nanocarriers [159]. Decreasing pH was found to increase the drug diffusion coefficient due to reduced water-doxorubicin and water-nanocarrier interactions. Simulations of doxorubicin adsorption on the GO surface and its release at neutral and acidic pH values showed that neutral blood pH values would be favourable for loading whilst release was facilitated at acidic pH levels in the extracellular tumour space.

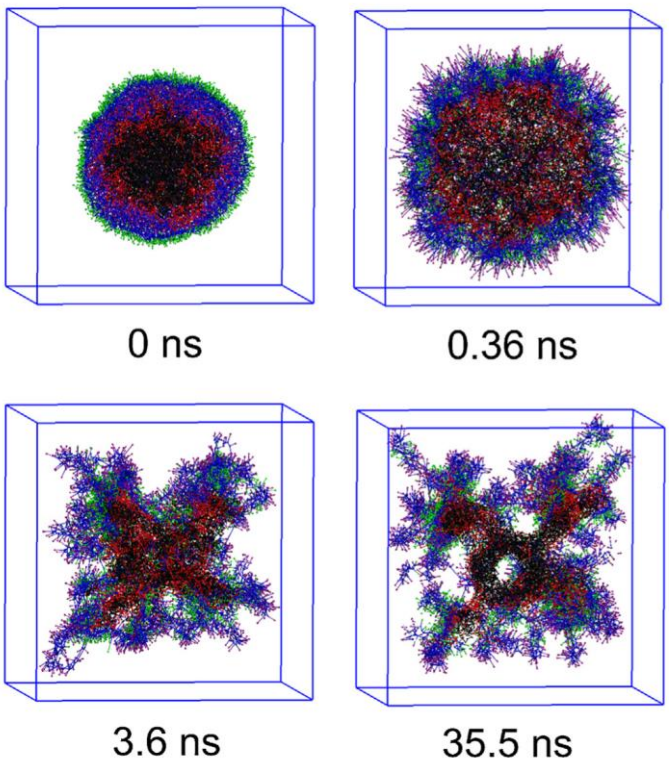

Fig. 11. Doxorubicin release behaviour from PCL-PDEA-PSBMA micelles in a system with pH of 5.0. Doxorubicin molecules are shown in black. PCL, PDEA and PEGMA are represented by the colours red, purple and green respectively. Reprint from Ref [156], with permission from Elsevier.

6. Modelling of implantable drug release devices

Implantable delivery systems are designed for targeted therapy through direct delivery of chemotherapeutics into tumour ECS. Cellular uptake is expected to be more effective due to enhanced drug exposure in the targeted region. However, implantation of such a device usually involves surgery which may alter the morphological and physiological conditions of the intratumoural microenvironment, thereby influencing drug transport and accumulation.

6.1. Chemotherapeutic wafers

Polymeric wafer implants have been used to provide chemotherapy for brain tumours. Loaded with chemotherapy drugs, they are implanted during brain surgery when the tumour is partially or completely removed. As it can release drug directly in the affected region, wafer implant has become a promising approach to bypass the blood-brain barrier (BBB). Gliadel® wafer containing 3.85% carmustine was approved by FDA in 1996 to serve as an adjuvant therapy for high-grade malignant glioma [160], and it is still in clinical use for prolonged and localized treatment of recurrent gliomas [161, 162]. Recent studies have focused on enhancing drug penetration and improving treatment efficacy through optimising the wafer structure [163] and coated drugs [164], combination with other treatment approaches [165], and the development of alternative micro/nano-structured implants [166].

A number of mathematical models for chemotherapeutic polymer implants have been developed. Early models assumed that diffusion was the only mechanism for drug transport, while drug elimination was described by first-order kinetics [67]. Although this model represented a major simplification of a complex system, it was able to identify drugs that are most suitable for polymer implant delivery to the brain; these include molecules that are water-soluble, undergo slow elimination and are diffusible in the brain. Rapid permeation of active drug molecules into capillaries was identified as the most significant barrier for effective drug distribution by polymer implant delivery.

The aforementioned mathematical description was integrated into the framework of a distributed model to investigate the delivery of IgG [84] and carmustine [167] to primitive neuroectodermal tumours under systemic administration and wafer implant delivery. The isolated tumour geometry was reconstructed from medical images in 3-D. Modelling results demonstrated the advantage of wafer implants in achieving high drug concentration and deep penetration for improved delivery outcomes. Optimisation study showed that it would be preferable to implant the wafers in the variable tumour zone than near the necrotic core. By using a transport-based model, Tan *et al*. [168] examined the impact of drug release profile on wafer implant delivery of etanidazole, and they showed that a double drug burst device , as shown in **Fig. 12**, was able to improve the penetration depth and therapeutic efficacy as compared to a zero-order release device. Their subsequent study on the effect of surgical opening [169] demonstrated that the opening could enhance convection of interstitial fluid, resulting in heterogeneous drug distribution and reduced treatment efficacy. As the tumour geometry was isolated in these simulations, the interstitial fluid flow in the whole brain was neglected.

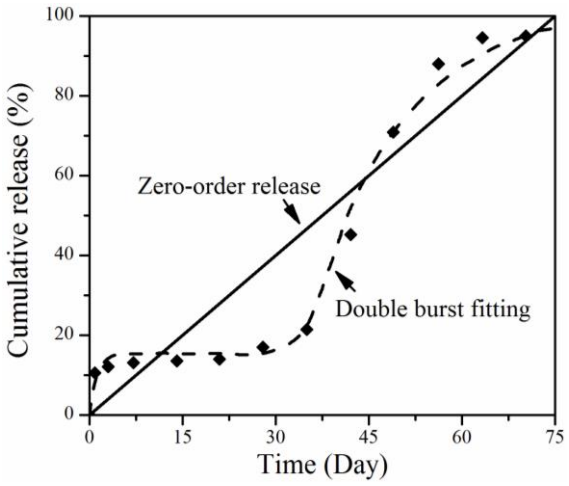

Fig. 12. Zero-order release profile and double burst release data with its mathematical fitting. The first burst is owing to drug diffusion from the wafer surface, while the second burst is resulted by wafer disintegration. Replot from Ref [168], with permission from John Wiley and Sons.

Arifin et al. developed a transport-based model to compare the delivery outcome of four different anticancer drugs to brain tumour with polymeric wafers [50]. When a quasi-steady state was reached,

their results showed that the effective concentration of paclitaxel was up to two orders of magnitude greater when compared to carmustine, 5-fluorouracil and methotrexate. However, there was no adequate drug deposition in regions near the ventricle. This study also showed that vascular renormalisation achieved with antiangiogenic treatment had little influence on drug distribution after surgical removal. In a separate study by Arifin et al. [85] the transport-based model was modified by dividing the tumour and normal tissue into three compartments, including the extracellular space, cell membrane and intracellular space. The free and bound drugs were initially described according to mass conservation, and then simplified by assuming equilibrium of free drug concentration among compartments and linear correlation between free and bound drugs. Computational analysis of BCNU wafer (Gliadel®) [85] was conducted to determine drug penetration and accumulation after implantation. As shown in **Fig. 13**, simulation results revealed that a quasi-steady state of drug transport could be reached within 1 day, while the drug concentration required for effective cell killing only lasted for less than a week. The drug penetration depth was limited to 2 mm from the wafer surface.

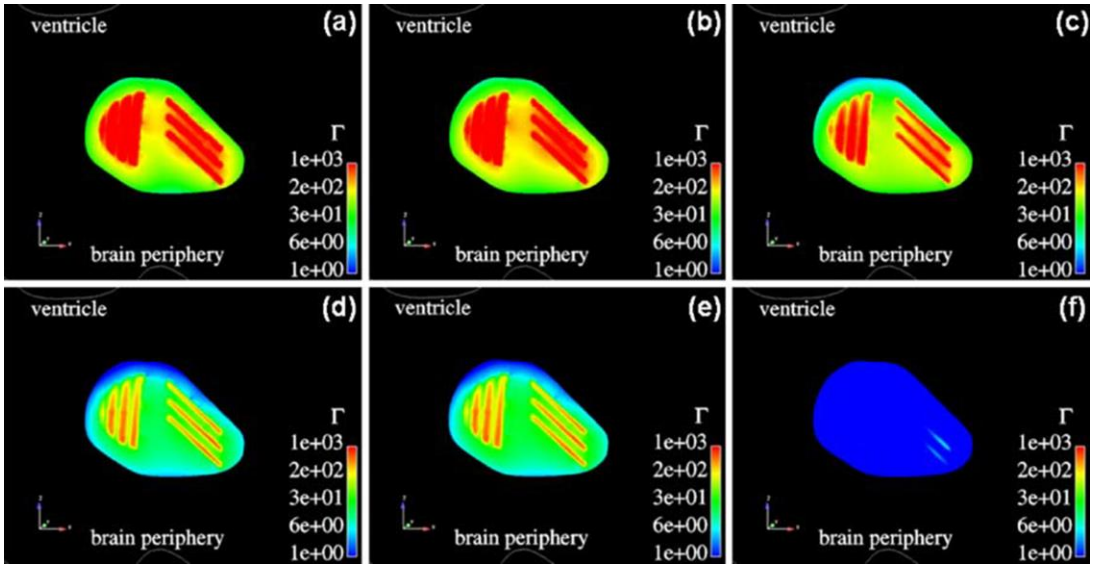

Fig. 13. Spatial distribution of carmustine delivered by wafers in tumour cavity at different time points, (a) Hour 4, (b) Hour 8, (c) Hour 24, (d) Hour 72, (e) Hour 120 and (f) Hour 168. Reprint from Ref [85], with permission from Springer Nature.

The influence of transient interstitial fluid flow on drug delivery after wafer implantation was studied using a 3-D brain tumour model reconstructed from MR images [170]. The model geometry contained viable tumour region, surgery-induced cavity and carmustine wafer. Governing equations for the interstitial fluid flow were solved first to generate the fluid pressure and velocity, which were then introduced into the drug transport equations to predict the distribution of carmustine. Simulation results demonstrated that the flow field, which was within creeping flow regime, could reach a quasi-

steady state within 3 hours after operation. Drug transport was temporarily enhanced by surgical removal of the tumour, but drug transport resistance generated by high intratumoural pressure could not be removed permanently by surgery alone.

Implantable hydrogel delivery of paclitaxel was simulated using a transport-based model for a 2-D brain tumour extracted from MR images [171]. Although paclitaxel hydrogel could achieve a similar penetration depth of 1-2 mm from carmustine wafers, the effective concentration of paclitaxel sustained much longer. It was also found that the hydrogel surface area to volume ratio was an important factor in determining a sustainable release.

Efforts have also been made to account for other relevant features, such as oedema which can occur as a result of trauma after surgical operations. The effects of oedema on drug transport were investigated on a 2-D model of the brain [172], wherein an extended form of Darcy's law was adopted together with differential transport properties in grey and white matter. The modelling results showed that oedema could increase IFP and that drug transport was more efficient in white matter owing to its more organised arrangement of nerve fibres (hence reduced tissue resistance) than in grey matter. Another numerical study [170] showed the same effect of oedema on IFP and enhanced interstitial fluid velocity; the latter contributed to increased drug concentration in normal brain tissue and the risk of side effects. Owing to the lack of *in vivo* data available for model set up [170], the cause of accelerated fluid loss was lumped into the hydraulic conductivity, without specifying changes in osmotic pressure, interstitial fluid pressure and intravascular pressure. The original location of oedema was another uncertainty in the simulation. This was either chosen randomly in the computational domain [173] or assumed to only form in the remnant tumour which was not removed during surgery [170]. Information on the exact location of initial oedema formation would help improve the accuracy of model predictions.

6.2. Convection-enhanced delivery

Convection-enhanced delivery (CED) has been designed to overcome the difficulties associated with drug transport cross the BBB. This is achieved through a catheter-needle system whereby pharmacological agents are directly injected into the tumour site. Drug transport is enhanced by the improved bulk movement of interstitial fluid, promoting deeper penetration in the tumour.

A systematic approach combining medical imaging and a tissue scale drug transport model was developed in an attempt to optimise the catheter design and infusion parameters for maximum drug penetration and tissue coverage in the target tumour [174]. The model employed the conservation equations for mass, momentum, and species transport, with different transport properties in white and grey matter based on medical images. It was found that catheter diameter, the number of holes and the location of infusion site had a strong influence on drug penetration depth and overall distribution

volume. Although this study was limited to 2-D brain slices, the proposed computational methodology could be extended to 3-D for patient-specific analysis.

Tumour tissues are known to have heterogeneous and anisotropic properties, and diffusion tensor MR images have been used to estimate anisotropic drug diffusivity and tissue hydraulic conductivity [93]. Simulations accounting for anisotropic properties were conducted on 3-D models of the rat ventral hippocampus reconstructed from MR images using a voxelized modelling approach [175]. Predicted albumin tracer distributions were compared with the corresponding MR measurements, showing similar patterns at the end of 10 μL infusion. Key transport features captured by the model included confinement of albumin tracer in ventral hippocampus structures with limited penetration into adjacent grey matter where fluid resistance is relatively high, and leakage into adjacent cerebrospinal fluid regions towards the end of CED infusion.

Tracer transport in a hind-limb tumour upon CED was examined using a 3-D transport-based model [176], where tissue hydraulic conductivity and drug diffusivity were correlated to the tissue porosity derived from MR images. Results showed that tracer concentration within the tumour rose exponentially to a maximum steady-state value upon continuous infusion, whereas the spatial distribution was asymmetric owing to non-uniform tissue properties. Sensitivity analysis concluded that infusing the tracer at tumour centre resulted in maximum tumour coverage and minimal leakage. The volume of distribution was found to be inversely related to the tissue hydraulic conductivity.

The effect of infusion parameter on intrathecal drug delivery was investigated using a computational model which employed a species transport equation incorporating infusion rate, drug diffusion, accumulation in tissue ECS and cerebrospinal fluid flow governed by Navier-Stokes equations [177]. Simulation results showed that multi-bolus infusion tended to cause drug localisation in the thoracic and cervical region, while single bolus injection and continuous drug infusion would be preferred for targeting the lumber spine. However, this model did not include the effects of vascular redistribution and cellular uptake.

Convection-enhanced delivery of carmustine and paclitaxel was examined using a realistic model for an intact brain tumour and a remnant brain tumour after surgical removal [178]. The shape of tumour and its surrounding normal tissue were reconstructed from MR images, and computational simulations were performed to compare the delivery outcomes under various operating conditions. Results showed that drug penetration could be improved by increasing either the drug concentration or the infusion rate for a given dosage. As compared to carmustine, paclitaxel was more sensitive to convective flow, and deeper penetration could be achieved by injecting paclitaxel at a location near the brain ventricle. In addition, simulations of increased drug diffusivity upon application of ultrasound at the infusion site showed improved drug penetration and accumulation for both carmustine and paclitaxel.

In the aforementioned models, interstitial fluid flow and drug transport were solved on a rigid porous domain without considering infusion-induced tissue deformation. In reality, the infused fluid is able to push the tissue to the direction against the catheter wall, leading to the formation of an annular cavity surrounding the catheter surface. The cavity is filled with infusate which can flow along the catheter track into the normal tissue, causing backflow. Infusion-induced backflow has been one of the major limitations for CED to be applied in clinical practice. Its effect on drug distribution has been examined using a poroelastic model, where the tissue was simplified as a linear elastic material and the colour function method was used to track the movement front of nanofluid [179]. Variations of local tissue porosity (φ) and tissue permeability (κ) were associated with tissue deformation. Results obtained on an idealised axisymmetric geometry demonstrated that backflow was a critical factor in determining the irregular distribution of nanoparticles. The length of backflow zone increased with the infusion rate and catheter diameter. It was also found that CED infusion was able to increase the tissue porosity near the catheter tip, easing drug penetration into the tumour.

A coupled poroelastic and drug transport model was developed to study CED-induced tissue deformation and drug distribution in a realistic brain model [180]. The white matter and grey matter were differentiated based on fractional anisotropy, diffusion tensor MR images were used to determine the orientation of fibre tracts in white matter and to calibrate anisotropic tissue permeability and drug diffusivity by following the procedure developed by Linninger *et al.* [93]. The model predicted preferential flow along the fibre tracts of white matter and changes in porosity and permeability. The predicted change in tissue porosity was small owing to the assumption of linear deformation; hence nonlinear models should be adopted for potential large porosity changes in future studies.

7. Model validation

All the drug transport models described in this review article involve some degree of assumptions which are usually introduced either to make the problem computationally tractable or to focus on the key interplays between chemotherapeutics and the biological system. Therefore, it is important to evaluate the performance and predictive power of each model. This can be achieved by qualitative and quantitative comparisons with established theoretical solutions, reliable measurements obtained in well-designed laboratory, *in vitro* experiments, or *in vivo* data.

Given that a typical solid tumour is at least two orders of magnitude larger than the inter-capillary distance, most of the macroscopic transport models treat tumour and its normal tissue as porous media with the interstitial fluid flow being described by Darcy's law. The original model proposed by Baxter and Jain predicted interstitial fluid velocity of 0.17 μm/s [51] which was well within the range of 0.13~0.2 μm/s measured in experiments [181]. The same modelling equations have been applied to 3-D realistic tumours, and the predicted interstitial fluid pressures [85, 88, 106] were well within the

experimental ranges of -3-6 mmHg and 8-30 mmHg for normal tissue and solid tumour, respectively [182, 183].

A limited number of studies have reported comparisons of computed drug distributions with experimental measurements. Arifin *et al.* simulated the delivery of carmustine to brain tumour by wafer implantation, and their predicted drug penetration was comparable to the corresponding *in vivo* data [85]. Ranganath *et al.* fabricated novel micro/nanostructured implants for paclitaxel delivery, and compared *in vivo* drug penetration in mouse brain with predictions obtained with a simplified transport model assuming 1-D steady diffusion/reaction [166]. As shown in **Fig. 14**, the model predictions and *in vivo* measurements revealed a qualitatively similar trend that drug concentration declined exponentially with the distance from the implant surface, suggesting that maintaining sufficient drug concentration at the implant site would be essential for achieving deeper drug penetration.

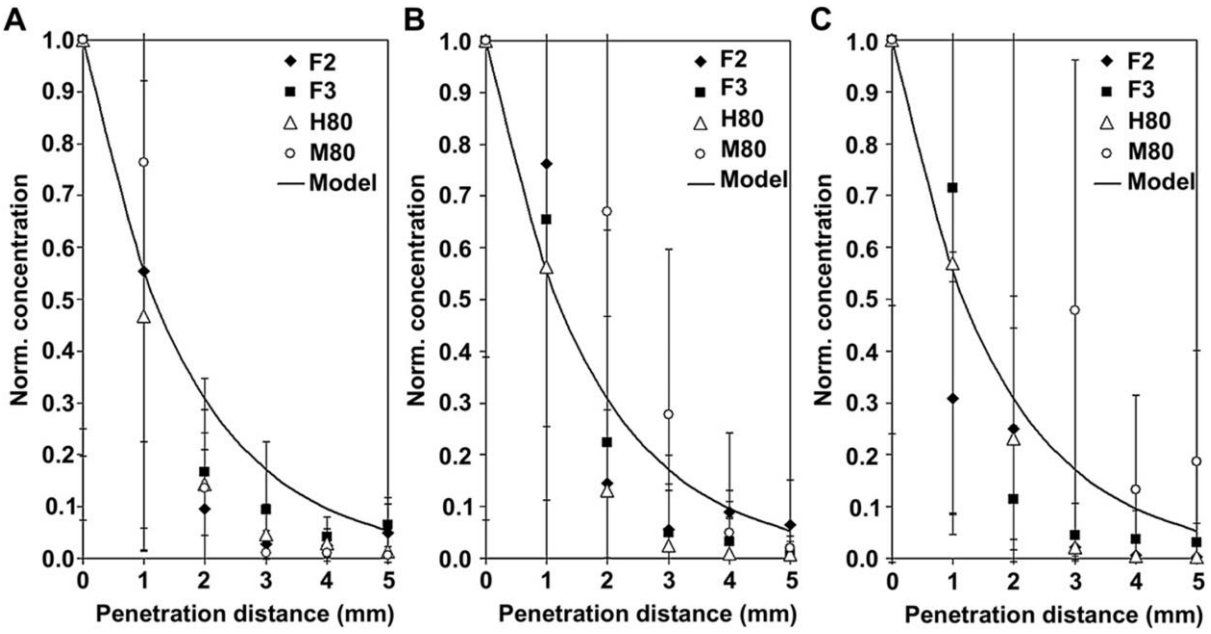

Fig. 14. Drug penetration profiles in the interstitial space for paclitaxel-loaded PLGA implants with different formulations (F2, F3, H80, M80) on (A) Day 14, (B) Day 28 and (C) Day 42. The model prediction (solid line) is compared to experimental measurement (dots) under the assumption of steady diffusion/reaction transport mechanism. Reprint from Ref [166], with permission from Elsevier.

Neeves *et al.* studied microfluidic probes for convection-enhanced drug delivery, and their model-predicted delivery volumes of Evans Blue and albumin were consistent with the corresponding experimental measurements with coefficients of multiple determination (R^2) of 0.7 and 0.83, respectively [185]. A multiphasic model describing brain tissue deformation, interstitial fluid flow and nanoparticle transport in convection-enhanced delivery was validated against gel-based experiments, showing similar nanofluid distribution patterns [179]. More recently, the performance of macroscopic transport-based model in predicting convection-enhanced delivery of nanoparticles was evaluated by

Zhan *et al.*, who showed that the predicted time variation of delivery volume was in good quantitative agreement with the experimental data obtained in animal studies [178]. The transport of MR tracer Gd-DTPA in human brain was simulated using a continuum transport model, which incorporated realistic heterogeneous tumour vasculature and accurate arterial input function obtained from patient-specific images [184]. The predicted tracer accumulation was compared to that derived from dynamic contrast-enhanced MRI, presenting similar spatial distributions as shown in **Fig. 15.**

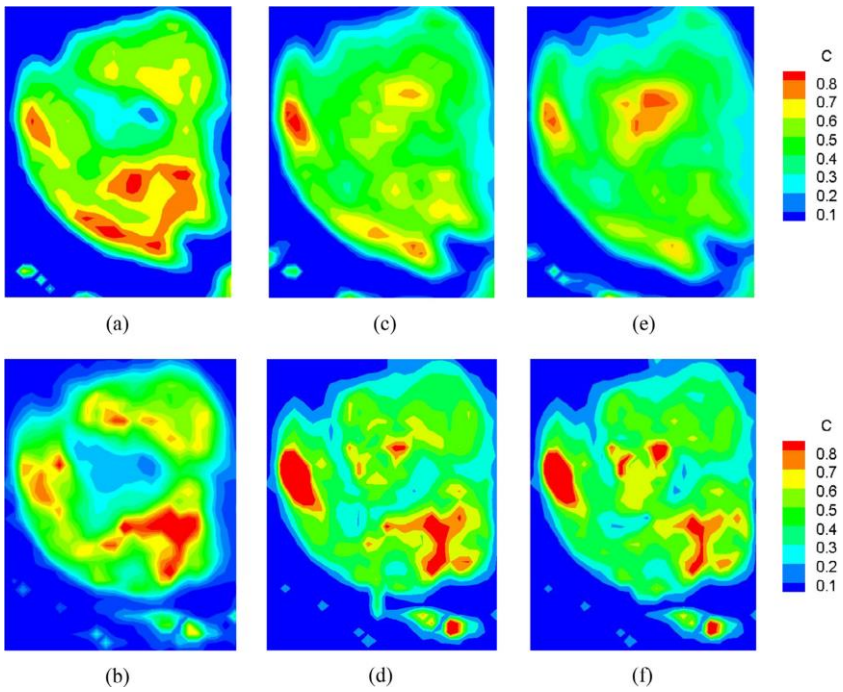

Fig. 15. Comparison of tracer concentration (mmol/L) from experimental measurement (top row) and computational predication (bottom row) at 3 min (a, b), 8 min (c, d) and 13 min (e, f). Reprint from Ref [184], with permission from Elsevier.

Validating mathematical models for chemotherapeutic drug transport and predictions of treatment outcomes remains a significant challenge. On the one hand, clinical evaluation of tumour inhibition or progression is often based on changes in tumour size over time, but existing tissue-scale, transport-based models cannot predict tumour regression or growth over a realistic time period required to cause a measurable change in tumour volume. On the other hand, tumour biological properties and drug transport properties are heterogeneous and anisotropic, which depend strongly on the tumour location, type and growth stage [46, 186-188]. Owing to the difficulty in accurately determining these properties on a patient-specific basis, average and representative values are adopted in most computational models. Although drug concentration appears to be a direct parameter that could be used for validation, comparisons of model prediction and experiment are usually made on *in vitro* models, or limited to qualitative trend rather than quantitative values. This is because *in vivo* measurement of drug concentration, especially its spatial distribution in tumour tissue is not yet

possible with existing non-invasive imaging techniques. Therefore, spatial-averaged values are often used for a coarse comparison. With the development of novel imaging techniques [189, 190], monitoring of chemotherapeutics distributions can be improved in the future.

8. Challenges and future perspectives

Cancer is a condition where cells grow and reproduce in an uncontrollable manner. It is recognised as a highly heterogeneous pathology with abnormality in morphology and functions, and dysregulations of pathways that govern the cell processes [191]. The delivery of chemotherapeutics to a solid tumour involves multiple physiological and physicochemical steps that are interconnected. Most existing transport-based models include the steps that are deemed important while ignoring the others, and there are varying degrees of uncertainties in model parameterisation. For this reason, most models are able to predict the qualitative trend of spatial and temporal concentration profiles of chemotherapeutic drugs, but their use for accurate, quantitative predictions is not yet established. Although considerable effort has been made in this regard, as described in this review, rigorous validations against *in vitro* and *in vivo* experiments are still lacking.

Mathematical modelling also provides a useful tool for the development and design of drug delivery systems (DDS), such as nanoparticle drug carriers, polymeric drug release implants and catheter-needle systems for convection-enhanced delivery. The effectiveness of nanoparticle-based DDS depends largely on the drug loading capacity, stability of the nanoparticle in the blood stream and release profiles of the drug from the nanoparticles. MD simulations are particularly valuable in this regard, as they provide detailed information on the structure of drug carriers and their interactions with the drug in a range of chemical and physical conditions. MD studies can not only serve to compliment experiments by providing a microscopic and quantitative understanding of experimental observations, but also identify limiting factors in a given system and help optimise the formation of nanoparticles. We have reviewed some of the literature where MD studies involving atomistic, CG and DPD methods were applied to study anti-cancer DDS. Atomistic MD methods are confined to time and length scales of several microseconds and nanometers, whereas CG and DPD methods are suitable for simulations on the scale of several hundred microseconds and sub-micron by neglecting atomistic details of the drug and its carrier. Hybrid atomistic and CG methods offer a promising solution to the scale issue by taking full advantage of both methods. Whilst loading and stability of the nanoparticles are important factors in developing DDS, a crucial process that is often overlooked in MD studies is the interaction of drug loaded nanoparticles with biological membranes. Such studies can provide a deeper understanding into the mechanisms of how nanoparticles can help transport drugs across cancer cell membranes. Increasing computational resources in recent years have opened the door for MD studies of DDS. We envisage the work in this field will grow rapidly as resources continue to increase and modelling systems become more efficient and realistic.

One of the outstanding challenges for continuum transport-based modelling is how to adequately describe the tumour microenvironment in tissue-scale models. Solid tumours are heterogeneous in nature with properties that vary from patient to patient owing to the genetic components involved in cancer development. Recent advances in medical imaging methods may hold some promise in providing tumour-specific physical and biological properties. Currently, however, most high-resolution imaging techniques are not suitable for *in vivo* applications and hence are unable to provide a detailed picture of the microscopic processes of the tumour microenvironment. Further efforts should also be made on developing an efficient multiscale platform that couples microscopic description and macroscopic transport processes in order to predict the influence of tumour-specific microenvironment on drug distribution in a realistic tumour.

Finally, the need for patient-specific modelling should be highlighted. This will require patient data at initial diagnosis and multiple follow-ups, including high-resolution medical images, clinical information and basic biochemical data. Incorporating such information into a computational model will allow personalised simulations which could be used to design effective therapies [7]. In the future, clinical systems for patient treatment planning and post-operation care may benefit from personalised simulations [192, 193, 194]. For this purpose, complex models with prohibitive computational requirement may not appear attractive. Reduced order models with input containing patient-specific information may be useful in providing preliminary predictions of treatment efficacy. However, cautions must be exercised in that the system is highly non-linear which can develop multiple resistances to drug therapy. Therefore, a large amount of experimental data is necessary to continuously develop such models with sufficiently high accuracy.

Parameters

C	Concentration
D	Diffusivity
p	Pressure
P	Permeability
T	Temperature
t	time
V	Volume

Subscripts

BD	Drugs bound with proteins
BP	Blood plasma
ECS	Extracellular space
FD	Free drugs
ICS	Intracellular space
IVS	Intravascular space
NP	Nanoparticle encapsulated drug
NT	Normal tissue
TU	Tumour/normal tissue

References

[1] M. Egeblad, E.S. Nakasone, Z. Werb, Tumors as organs: complex tissues that interface with the entire organism, Developmental Cell, 18 (2010) 884-901.

[2] P. Baluk, H. Hashizume, D.M. McDonald, Cellular abnormalities of blood vessels as targets in cancer, Current Opinion in Genetics & Development, 15 (2005) 102-111.

[3] C.-H. Heldin, K. Rubin, K. Pietras, A. Östman, High interstitial fluid pressure—an obstacle in cancer therapy, Nature Reviews Cancer, 4 (2004) 806-813.

[4] J.L.-S. Au, B.Z. Yeung, M.G. Wientjes, Z. Lu, M.G. Wientjes, Delivery of cancer therapeutics to extracellular and intracellular targets: determinants, barriers, challenges and opportunities, Advanced Drug Delivery Reviews, 97 (2016) 280-301.

[5] C. Liu, J. Krishnan, J. Stebbing, X.Y. Xu, Use of mathematical models to understand anticancer drug delivery and its effect on solid tumors, Pharmacogenomics, 12 (2011) 1337-1348.

[6] C.M. Groh, M.E. Hubbard, P.F. Jones, P.M. Loadman, N. Periasamy, B.D. Sleeman, S.W. Smye, C.J. Twelves, R.M. Phillips, Mathematical and computational models of drug transport in tumours, Journal of the Royal Society Interface, 11 (2014) 20131173.

[7] A. Karolak, D.A. Markov, L.J. McCawley, K.A. Rejniak, Towards personalized computational oncology: from spatial models of tumour spheroids, to organoids, to tissues, Journal of the Royal Society Interface, 15 (2018) 20170703.

[8] Q. Zhou, J.M. Gallo, The pharmacokinetic/pharmacodynamic pipeline: translating anticancer drug pharmacology to the clinic, The AAPS Journal, 13 (2011) 111-120.

[9] M. Danhof, E.C. de Lange, O.E. Della Pasqua, B.A. Ploeger, R.A. Voskuyl, Mechanism-based pharmacokinetic-pharmacodynamic (PK-PD) modeling in translational drug research, Trends in Pharmacological Sciences, 29 (2008) 186-191.

[10] H.-J. Kuh, S.H. Jang, M.G. Wientjes, J.L.-S. Au, Computational model of intracellular pharmacokinetics of paclitaxel, Journal of Pharmacology and Experimental Therapeutics, 293 (2000) 761-770.

[11] T. Puchalski, U. Prabhakar, Q. Jiao, B. Berns, H.M. Davis, Pharmacokinetic and pharmacodynamic modeling of an anti–interleukin-6 chimeric monoclonal antibody (siltuximab) in patients with metastatic renal cell carcinoma, Clinical Cancer Research, 16 (2010) 1652-1661.

[12] M. Battaglia, R. Parker, Pharmacokinetic/pharmacodynamic modelling of intracellular gemcitabine triphosphate accumulation: translating in vitro to in vivo, IET Systems Biology, 5 (2011) 34-43.

[13] J. Sharma, H. Lv, J.M. Gallo, Intratumoral modeling of gefitinib pharmacokinetics and pharmacodynamics in an orthotopic mouse model of glioblastoma, Cancer Research, 73 (2013) 5242-5252.

[14] J.W. Yates, S.V. Holt, A. Logie, K. Payne, K. Woods, R.W. Wilkinson, B.R. Davies, S.M. Guichard, A Pharmacokinetic-Pharmacodynamic model predicting tumour growth inhibition after intermittent administration with the mTOR kinase inhibitor AZD8055, British Journal of Pharmacology, 174 (2017) 2652-2661.

[15] H. Harashima, M. Tsuchihashi, S. Iida, H. Doi, H. Kiwada, Pharmacokinetic/pharmacodynamic modeling of antitumor agents encapsulated into liposomes, Advanced Drug Delivery Reviews, 40 (1999) 39-61.

[16] D. Ribeiro, J.M. Pinto, An integrated network-based mechanistic model for tumor growth dynamics under drug administration, Computers in Biology and Medicine, 39 (2009) 368-384.

[17] R. O'Connor, M. Clynes, P. Dowling, N. O'Donovan, L. O'Driscoll, Drug resistance in cancer–searching for mechanisms, markers and therapeutic agents, Expert Opinion on Drug Metabolism & Toxicology, 3 (2007) 805-817.

[18] C. Marbeuf-Gueye, M. Salerno, P. Quidu, A. Garnier-Suillerot, Inhibition of the P-glycoprotein-and multidrug resistance protein-mediated efflux of anthracyclines and calceinacetoxymethyl ester by PAK-104P, European Journal of Pharmacology, 391 (2000) 207-216.

[19] S.H. Jang, M.G. Wientjes, J.L.-S. Au, Kinetics of P-glycoprotein-mediated efflux of paclitaxel, Journal of Pharmacology and Experimental Therapeutics, 298 (2001) 1236-1242.

[20] K.T. Luu, J.A. Uchizono, P-glycoprotein induction and tumor cell-kill dynamics in response to differential doxorubicin dosing strategies: a theoretical pharmacodynamic model, Pharmaceutical Research, 22 (2005) 710-715.

[21] R. Venkatasubramanian, M.A. Henson, N.S. Forbes, Integrating cell-cycle progression, drug penetration and energy metabolism to identify improved cancer therapeutic strategies, Journal of Theoretical Biology, 253 (2008) 98-117.

[22] H.E. Skipper, The effects of chemotherapy on the kinetics of leukemic cell behavior, Cancer Research, 25 (1965) 1544-1550.

[23] S. Ozawa, Y. Sugiyama, Y. Mitsuhashi, T. Kobayashi, M. Inaba, Cell killing action of cell cycle phase-non-specific antitumor agents is dependent on concentration-time product, Cancer Chemotherapy and Pharmacology, 21 (1988) 185-190.

[24] L.M. Levasseur, H.K. Slocum, Y.M. Rustum, W.R. Greco, Modeling of the time-dependency of in vitro drug cytotoxicity and resistance, Cancer Research, 58 (1998) 5749-5761.

[25] S.N. Gardner, A mechanistic, predictive model of dose-response curves for cell cycle phase-specific and-nonspecific drugs, Cancer Research, 60 (2000) 1417-1425.

[26] A.W. El-Kareh, T.W. Secomb, A mathematical model for cisplatin cellular pharmacodynamics, Neoplasia, 5 (2003) 161-169.

[27] A.W. El-Kareh, R.E. Labes, T.W. Secomb, Cell cycle checkpoint models for cellular pharmacology of paclitaxel and platinum drugs, The AAPS Journal, 10 (2008) 15-34.

[28] C. Liu, J. Krishnan, X.Y. Xu, A systems-based mathematical modelling framework for investigating the effect of drugs on solid tumours, Theoretical Biology and Medical Modelling, 8 (2011) 45-65.

[29] C. Liu, J. Krishnan, X.Y. Xu, Intrinsic and induced drug resistance mechanisms: in silico investigations at the cellular and tissue scales, Integrative Biology, 7 (2015) 1044-1060.

[30] A. Bertuzzi, A. Gandolfi, Cell kinetics in a tumour cord, Journal of Theoretical Biology, 204 (2000) 587-599.

[31] S. Eikenberry, A tumor cord model for doxorubicin delivery and dose optimization in solid tumors, Theoretical Biology and Medical Modelling, 6 (2009) 16-35.

[32] A.W. El-Kareh, T.W. Secomb, A mathematical model for comparison of bolus injection, continuous infusion, and liposomal delivery of doxorubicin to tumor cells, Neoplasia, 2 (2000) 325-338.

[33] M.E. Hubbard, M. Jove, P.M. Loadman, R.M. Phillips, C.J. Twelves, S.W. Smye, Drug delivery in a tumour cord model: a computational simulation, Royal Society Open Science, 4 (2017) 170014.

[34] A.R. Anderson, M. Chaplain, Continuous and discrete mathematical models of tumor-induced angiogenesis, Bulletin of Mathematical Biology, 60 (1998) 857-899.

[35] A. Stephanou, S.R. McDougall, A.R. Anderson, M.A. Chaplain, Mathematical modelling of flow in 2D and 3D vascular networks: applications to anti-angiogenic and chemotherapeutic drug strategies, Mathematical and Computer Modelling, 41 (2005) 1137-1156.

[36] M. Sefidgar, M. Soltani, K. Raahemifar, M. Sadeghi, H. Bazmara, M. Bazargan, M.M. Naeenian, Numerical modeling of drug delivery in a dynamic solid tumor microvasculature, Microvascular Research, 99 (2015) 43-56.

[37] E. Kim, S. Stamatelos, J. Cebulla, Z.M. Bhujwalla, A.S. Popel, A.P. Pathak, Multiscale imaging and computational modeling of blood flow in the tumor vasculature, Annals of Biomedical Engineering, 40 (2012) 2425-2441.

[38] T. Secomb, R. Hsu, R. Braun, J. Ross, J. Gross, M. Dewhirst, Theoretical simulation of oxygen transport to tumors by three-dimensional networks of microvessels, Advances in Experimental Medicine and Biology, 454 (1998) 629-634.

[39] S.K. Stamatelos, E. Kim, A.P. Pathak, A.S. Popel, A bioimage informatics based reconstruction of breast tumor microvasculature with computational blood flow predictions, Microvascular Research, 91 (2014) 8-21.

[40] L. Cattaneo, P. Zunino, A computational model of drug delivery through microcirculation to compare different tumor treatments, International Journal for Numerical Methods in Biomedical Engineering, 30 (2014) 1347-1371.

[41] T.W. Secomb, A Green's function method for simulation of time-dependent solute transport and reaction in realistic microvascular geometries, Mathematical Medicine and Biology: A Journal of the IMA, 33 (2015) 475-494.

[42] V.P. Chauhan, T. Stylianopoulos, J.D. Martin, Z. Popovic, O. Chen, W.S. Kamoun, M.G. Bawendi, D. Fukumura, R.K. Jain, Normalization of tumour blood vessels improves the delivery of nanomedicines in a size-dependent manner, Nature Nanotechnology, 7 (2012) 383-388.

[43] T. Stylianopoulos, K. Soteriou, D. Fukumura, R.K. Jain, Cationic nanoparticles have superior transvascular flux into solid tumors: insights from a mathematical model, Annals of Biomedical Engineering, 41 (2013) 68-77.

[44] S.R. McDougall, A.R. Anderson, M.A. Chaplain, Mathematical modelling of dynamic adaptive tumour-induced angiogenesis: clinical implications and therapeutic targeting strategies, Journal of Theoretical Biology, 241 (2006) 564-589.

[45] G. Fullstone, J. Wood, M. Holcombe, G. Battaglia, Modelling the transport of nanoparticles under blood flow using an agent-based approach, Scientific Reports, 5 (2015) 10649.

[46] P.A. Netti, D.A. Berk, M.A. Swartz, A.J. Grodzinsky, R.K. Jain, Role of extracellular matrix assembly in interstitial transport in solid tumors, Cancer Research, 60 (2000) 2497-2503.

[47] R. Grantab, S. Sivananthan, I.F. Tannock, The penetration of anticancer drugs through tumor tissue as a function of cellular adhesion and packing density of tumor cells, Cancer Research, 66 (2006) 1033-1039.

[48] K.A. Rejniak, V. Estrella, T. Chen, A.S. Cohen, M. Lloyd, D.L. Morse, The role of tumor tissue architecture in treatment penetration and efficacy: an integrative study, Frontiers in Oncology, 3 (2013) 111-123.

[49] W. Zhan, W. Gedroyc, X. Yun Xu, Mathematical modelling of drug transport and uptake in a realistic model of solid tumour, Protein and Peptide Letters, 21 (2014) 1146-1156.

[50] D.Y. Arifin, K.Y.T. Lee, C.-H. Wang, Chemotherapeutic drug transport to brain tumor, Journal of Controlled Release, 137 (2009) 203-210.

[51] L.T. Baxter, R.K. Jain, Transport of fluid and macromolecules in tumors. I. Role of interstitial pressure and convection, Microvascular Research, 37 (1989) 77-104.

[52] L.T. Baxter, R.K. Jain, Transport of fluid and macromolecules in tumors. II. Role of heterogeneous perfusion and lymphatics, Microvascular Research, 40 (1990) 246-263.

[53] L.T. Baxter, R.K. Jain, Transport of fluid and macromolecules in tumors: III. Role of binding and metabolism, Microvascular Research, 41 (1991) 5-23.

[54] J. Sinek, H. Frieboes, X. Zheng, V. Cristini, Two-dimensional chemotherapy simulations demonstrate fundamental transport and tumor response limitations involving nanoparticles, Biomedical Microdevices, 6 (2004) 297-309.

[55] A.R. Tzafriri, E.I. Lerner, M. Flashner-Barak, M. Hinchcliffe, E. Ratner, H. Parnas, Mathematical modeling and optimization of drug delivery from intratumorally injected microspheres, Clinical Cancer Research, 11 (2005) 826-834.

[56] T.T. Goodman, J. Chen, K. Matveev, S.H. Pun, Spatio-temporal modeling of nanoparticle delivery to multicellular tumor spheroids, Biotechnology and Bioengineering, 101 (2008) 388-399.

[57] M.G. Wientjes, B.Z. Yeung, Z. Lu, M.G. Wientjes, J.L. Au, Predicting diffusive transport of cationic liposomes in 3-dimensional tumor spheroids, Journal of Controlled Release, 192 (2014) 10-18.

[58] Y.M. Goh, H.L. Kong, C.H. Wang, Simulation of the delivery of doxorubicin to hepatoma, Pharmaceutical Research, 18 (2001) 761-770.

[59] C. Liu, J. Krishnan, X.Y. Xu, Investigating the effects of ABC transporter-based acquired drug resistance mechanisms at the cellular and tissue scale, Integrative Biology, 5 (2013) 555-568.

[60] S. Gao, J. Singh, Effect of oleic acid/ethanol and oleic acid/propylene glycol on the in vitro percutaneous absorption of 5-fluorouracil and tamoxifen and the macroscopic barrier property of porcine epidermis, International Journal of Pharmaceutics, 165 (1998) 45-55.

[61] J.E. Wolff, S. Berrak, S.E. Koontz Webb, M. Zhang, Nitrosourea efficacy in high-grade glioma: a survival gain analysis summarizing 504 cohorts with 24193 patients, Journal of Neuro-oncology, 88 (2008) 57-63.

[62] D.K. Shah, B.S. Shin, J. Veith, K. Tóth, R.J. Bernacki, J.P. Balthasar, Use of an anti-vascular endothelial growth factor antibody in a pharmacokinetic strategy to increase the efficacy of intraperitoneal chemotherapy, Journal of Pharmacology and Experimental Therapeutics, 329 (2009) 580-591.

[63] J. Mei, Y. Cheng, Y. Song, Y. Yang, F. Wang, Y. Liu, Z. Wang, Experimental study on targeted methotrexate delivery to the rabbit brain via magnetic resonance imaging–guided focused ultrasound, Journal of Ultrasound in Medicine, 28 (2009) 871-880.

[64] J. Chen, F. Zehtabi, J. Ouyang, J. Kong, W. Zhong, M.M. Xing, Reducible self-assembled micelles for enhanced intracellular delivery of doxorubicin, Journal of Materials Chemistry, 22 (2012) 7121-7129.

[65] F. Petrelli, K. Borgonovo, S. Barni, Targeted delivery for breast cancer therapy: the history of nanoparticle-albumin-bound paclitaxel, Expert Opinion on Pharmacotherapy, 11 (2010) 1413-1432.

[66] L.K. Fung, M. Shin, B. Tyler, H. Brem, W.M. Saltzman, Chemotherapeutic drugs released from polymers: distribution of 1, 3-bis (2-chloroethyl)-l-nitrosourea in the rat brain, Pharmaceutical Research, 13 (1996) 671-682.

[67] W.M. Saltzman, M.L. Radomsky, Drugs released from polymers: diffusion and elimination in brain tissue, Chemical Engineering Science, 46 (1991) 2429-2444.

[68] T.-L. Hwang, C.-L. Fang, C.-H. Chen, J.-Y. Fang, Permeation enhancer-containing water-in-oil nanoemulsions as carriers for intravesical cisplatin delivery, Pharmaceutical Research, 26 (2009) 2314-2323.

[69] T. Formariz, V. Sarmento, A. Silva-Junior, M. Scarpa, C.V. Santilli, A. Oliveira, Doxorubicin biocompatible O/W microemulsion stabilized by mixed surfactant containing soya phosphatidylcholine, Colloids and Surfaces B: Biointerfaces, 51 (2006) 54-61.

[70] L.K. Fung, M.G. Ewend, A. Sills, E.P. Sipos, R. Thompson, M. Watts, O.M. Colvin, H. Brem, W.M. Saltzman, Pharmacokinetics of interstitial delivery of carmustine, 4-hydroperoxycyclophosphamide, and paclitaxel from a biodegradable polymer implant in the monkey brain, Cancer Research, 58 (1998) 672-684.

[71] D.S. Wishart, C. Knox, A.C. Guo, S. Shrivastava, M. Hassanali, P. Stothard, Z. Chang, J. Woolsey, DrugBank: a comprehensive resource for in silico drug discovery and exploration, Nucleic Acids Research, 34 (2006) D668-D672.

[72] W. Cole, W. Wolf, Preparation and metabolism of a cisplatin/serum protein complex, Chemico-biological Interactions, 30 (1980) 223-235.

[73] M. Maia, S. Saivin, E. Chatelut, M. Malmary, G. Houin, In vitro and in vivo protein binding of methotrexate assessed by microdialysis, International Journal of Clinical Pharmacology and Therapeutics, 34 (1996) 335-341.

[74] R.F. Greene, J.M. Collins, J.F. Jenkins, J.L. Speyer, C.E. Myers, Plasma pharmacokinetics of adriamycin and adriamycinol: implications for the design of in vitro experiments and treatment protocols, Cancer Research, 43 (1983) 3417-3421.

[75] W. Zhan, W. Gedroyc, X.Y. Xu, Effect of heterogeneous microvasculature distribution on drug delivery to solid tumour, Journal of Physics D: Applied Physics, 47 (2014) 475401.

[76] E.A. Swabb, J. Wei, P.M. Gullino, Diffusion and convection in normal and neoplastic tissues, Cancer Research, 34 (1974) 2814-2822.

[77] A. Buur, H. Bundgaard, Prodrugs of 5-fluorouracil. III. Hydrolysis kinetics in aqueous solution and biological media, lipophilicity and solubility of various 1-carbamoyl derivatives of 5-fluorouracil, International Journal of Pharmaceutics, 23 (1985) 209-222.

[78] P.B. Layton, H.S. Greenberg, P.L. Stetson, W.D. Ensminger, J.W. Gyves, BCNU solubility and toxicity in the treatment of malignant astrocytomas, Journal of Neurosurgery, 60 (1984) 1134-1137.

[79] W.-P. Liu, Q.-S. Ye, Y. Yu, X.-Z. Chen, S.-Q. Hou, L.-G. Lou, Y.-P. Yang, Y.-M. Wang, Q. Su, Novel lipophilic platinum (II) compounds of salicylate derivatives, Platinum Metals Review, 52 (2008) 163-171.

[80] I.V. Tetko, J. Gasteiger, R. Todeschini, A. Mauri, D. Livingstone, P. Ertl, V.A. Palyulin, E.V. Radchenko, N.S. Zefirov, A.S. Makarenko, Virtual computational chemistry laboratory–design and description, Journal of Computer-aided Molecular Design, 19 (2005) 453-463.

[81] R.T. Liggins, W. Hunter, H.M. Burt, Solid-state characterization of paclitaxel, Journal of Pharmaceutical Sciences, 86 (1997) 1458-1463.

[82] C.M. Hand, J.R. Vender, P. Black, Chemotherapy in experimental brain tumor, part 1: in vitro colorimetric MTT assay, Journal of Neuro-oncology, 36 (1998) 1-6.

[83] D.J. Kerr, A.M. Kerr, R.I. Freshney, S.B. Kaye, Comparative intracellular uptake of adriamycin and 4'-deoxydoxorubicin by nonsmall cell lung tumor cells in culture and its relationship to cell survival, Biochemical Pharmacology, 35 (1986) 2817-2823.

[84] C.-H. Wang, J. Li, Three-dimensional simulation of IgG delivery to tumors, Chemical Engineering Science, 53 (1998) 3579-3600.

[85] D.Y. Arifin, K.Y.T. Lee, C.-H. Wang, K.A. Smith, Role of convective flow in carmustine delivery to a brain tumor, Pharmaceutical Research, 26 (2009) 2289-2302.

[86] M. Sefidgar, M. Soltani, K. Raahemifar, H. Bazmara, S.M.M. Nayinian, M. Bazargan, Effect of tumor shape, size, and tissue transport properties on drug delivery to solid tumors, Journal of Biological Engineering, 8 (2014) 12.

[87] W. Zhan, W. Gedroyc, X.Y. Xu, The effect of tumour size on drug transport and uptake in 3-D tumour models reconstructed from magnetic resonance images, PloS One, 12 (2017) e0172276.

[88] J. Zhao, H. Salmon, M. Sarntinoranont, Effect of heterogeneous vasculature on interstitial transport within a solid tumor, Microvascular Research, 73 (2007) 224-236.

[89] M. Bilgen, P.A. Narayana, A pharmacokinetic model for quantitative evaluation of spinal cord injury with dynamic contrast-enhanced magnetic resonance imaging, Magnetic Resonance in Medicine, 46 (2001) 1099-1106.

[90] A. Bhandari, A. Bansal, A. Singh, N. Sinha, Transport of Liposome Encapsulated Drugs in Voxelized Computational Model of Human Brain Tumors, IEEE Transactions on NanoBioscience, 16 (2017) 634-644.

[91] M. Avellaneda, S. Torquato, Rigorous link between fluid permeability, electrical conductivity, and relaxation times for transport in porous media, Physics of Fluids A: Fluid Dynamics, 3 (1991) 2529-2540.

[92] P.J. Basser, C. Pierpaoli, Microstructural and physiological features of tissues elucidated by quantitative-diffusion-tensor MRI, Journal of Magnetic Resonance, 213 (2011) 560-570.

[93] A.A. Linninger, M.R. Somayaji, T. Erickson, X. Guo, R.D. Penn, Computational methods for predicting drug transport in anisotropic and heterogeneous brain tissue, Journal of Biomechanics, 41 (2008) 2176-2187.

[94] W. Zhan, C.-H. Wang, Convection enhanced delivery of chemotherapeutic drugs into brain tumour, Journal of Controlled Release, 271 (2018) 74-87.

[95] M. Soltani, P. Chen, Effect of tumor shape and size on drug delivery to solid tumors, Journal of Biological Engineering, 6 (2012) 4-18.

[96] T. Nhan, A. Burgess, L. Lilge, K. Hynynen, Modeling localized delivery of Doxorubicin to the brain following focused ultrasound enhanced blood-brain barrier permeability, Physics in Medicine and Biology, 59 (2014) 5987-6004.

[97] Z. Li, S. Tan, S. Li, Q. Shen, K. Wang, Cancer drug delivery in the nano era: An overview and perspectives, Oncology Reports, 38 (2017) 611-624.

[98] S.Y. Madani, N. Naderi, O. Dissanayake, A. Tan, A.M. Seifalian, A new era of cancer treatment: carbon nanotubes as drug delivery tools, International Journal of Nanomedicine, 6 (2011) 2963–2979.

[99] Z. Liu, J.T. Robinson, S.M. Tabakman, K. Yang, H. Dai, Carbon materials for drug delivery & cancer therapy, Materials Today, 14 (2011) 316-323.

[100] T. Sun, Y.S. Zhang, B. Pang, D.C. Hyun, M. Yang, Y. Xia, Engineered nanoparticles for drug delivery in cancer therapy, Angewandte Chemie International Edition, 53 (2014) 12320-12364.

[101] L. Zha, B. Banik, F. Alexis, Stimulus responsive nanogels for drug delivery, Soft Matter, 7 (2011) 5908-5916.

[102] F. Danhier, O. Feron, V. Préat, To exploit the tumor microenvironment: passive and active tumor targeting of nanocarriers for anti-cancer drug delivery, Journal of Controlled Release, 148 (2010) 135-146.

[103] A. Gasselhuber, M.R. Dreher, F. Rattay, B.J. Wood, D. Haemmerich, Comparison of conventional chemotherapy, stealth liposomes and temperature-sensitive liposomes in a mathematical model, PLoS One, 7 (2012) e47453.

[104] C. Liu, X.Y. Xu, A systematic study of temperature sensitive liposomal delivery of doxorubicin using a mathematical model, Computers in Biology and Medicine, 60 (2015) 107-116.

[105] A. Zhang, X. Mi, G. Yang, L.X. Xu, Numerical study of thermally targeted liposomal drug delivery in tumor, Journal of Heat Transfer, 131 (2009) 043209.

[106] W. Zhan, X.Y. Xu, A mathematical model for thermosensitive liposomal delivery of Doxorubicin to solid tumour, Journal of Drug Delivery, 2013 (2013) 172529.

[107] A. Gasselhuber, M.R. Dreher, A. Partanen, P.S. Yarmolenko, D. Woods, B.J. Wood, D. Haemmerich, Targeted drug delivery by high intensity focused ultrasound mediated hyperthermia combined with temperature-sensitive liposomes: computational modelling and preliminary in vivo validation, International Journal of Hyperthermia, 28 (2012) 337-348.

[108] W. Zhan, Mathematical modelling of drug delivery to solid tumour, Imperial College London, 2014.

[109] N.J. McDannold, R.L. King, F.A. Jolesz, K.H. Hynynen, Usefulness of MR imaging-derived thermometry and dosimetry in determining the threshold for tissue damage induced by thermal surgery in rabbits, Radiology, 216 (2000) 517-523.

[110] L. Curiel, F. Chavrier, B. Gignoux, S. Pichardo, S. Chesnais, J. Chapelon, Experimental evaluation of lesion prediction modelling in the presence of cavitation bubbles: intended for high-intensity focused ultrasound prostate treatment, Medical and Biological Engineering and Computing, 42 (2004) 44-54.

[111] W.L. Lin, R. Roemer, K. Hynynen, Theoretical and experimental evaluation of a temperature controller for scanned focused ultrasound hyperthermia, Medical Physics, 17 (1990) 615-625.

[112] R. Staruch, R. Chopra, K. Hynynen, Localised drug release using MRI-controlled focused ultrasound hyperthermia, International Journal of Hyperthermia, 27 (2011) 156-171.

[113] H. O'Neil, Theory of focusing radiators, The Journal of the Acoustical Society of America, 21 (1949) 516-526.

[114] M.A. Solovchuk, T.W. Sheu, W.-L. Lin, I. Kuo, M. Thiriet, Simulation study on acoustic streaming and convective cooling in blood vessels during a high-intensity focused ultrasound thermal ablation, International Journal of Heat and Mass Transfer, 55 (2012) 1261-1270.

[115] M.A. Solovchuk, T.W. Sheu, M. Thiriet, W.-L. Lin, On a computational study for investigating acoustic streaming and heating during focused ultrasound ablation of liver tumor, Applied Thermal Engineering, 56 (2013) 62-76.

[116] T.W. Sheu, M.A. Solovchuk, A.W. Chen, M. Thiriet, On an acoustics–thermal–fluid coupling model for the prediction of temperature elevation in liver tumor, International Journal of Heat and Mass Transfer, 54 (2011) 4117-4126.

[117] R.J. McGough, T.V. Samulski, J.F. Kelly, An efficient grid sectoring method for calculations of the near-field pressure generated by a circular piston, The Journal of the Acoustical Society of America, 115 (2004) 1942-1954.

[118] R.J. McGough, Rapid calculations of time-harmonic nearfield pressures produced by rectangular pistons, The Journal of the Acoustical Society of America, 115 (2004) 1934-1941.

[119] X. Zeng, R.J. McGough, Evaluation of the angular spectrum approach for simulations of near-field pressures, The Journal of the Acoustical Society of America, 123 (2008) 68-76.

[120] X. Zeng, R.J. McGough, Optimal simulations of ultrasonic fields produced by large thermal therapy arrays using the angular spectrum approach, The Journal of the Acoustical Society of America, 125 (2009) 2967-2977.

[121] G. Clement, K. Hynynen, Field characterization of therapeutic ultrasound phased arrays through forward and backward planar projection, The Journal of the Acoustical Society of America, 108 (2000) 441-446.

[122] D. Chen, R.J. McGough, A 2D fast near-field method for calculating near-field pressures generated by apodized rectangular pistons, The Journal of the Acoustical Society of America, 124 (2008) 1526-1537.

[123] V. Torchilin, Targeted polymeric micelles for delivery of poorly soluble drugs, Cellular and Molecular Life Sciences CMLS, 61 (2004) 2549-2559.

[124] S. Parveen, S.K. Sahoo, Polymeric nanoparticles for cancer therapy, Journal of Drug Targeting, 16 (2008) 108-123.

[125] U. Kedar, P. Phutane, S. Shidhaye, V. Kadam, Advances in polymeric micelles for drug delivery and tumor targeting, Nanomedicine: Nanotechnology, Biology and Medicine, 6 (2010) 714-729.

[126] S. Biswas, P. Kumari, P.M. Lakhani, B. Ghosh, Recent advances in polymeric micelles for anti-cancer drug delivery, European Journal of Pharmaceutical Sciences, 83 (2016) 184-202.

[127] M. De Vivo, M. Masetti, G. Bottegoni, A. Cavalli, Role of molecular dynamics and related methods in drug discovery, Journal of Medicinal Chemistry, 59 (2016) 4035-4061.

[128] R. Friedman, K. Boye, K. Flatmark, Molecular modelling and simulations in cancer research, Biochimica et Biophysica Acta (BBA)-Reviews on Cancer, 1836 (2013) 1-14.

[129] H.A. Karimi-Varzaneh, F. Müller-Plathe, Coarse-grained modeling for macromolecular chemistry, Multiscale Molecular Methods in Applied Chemistry, 307 (2011), 295-321.

[130] E. Moeendarbary, T. Ng, M. Zangeneh, Dissipative particle dynamics: introduction, methodology and complex fluid applications—a review, International Journal of Applied Mechanics, 1 (2009) 737-763.

[131] M. Ramezanpour, S. Leung, K. Delgado-Magnero, B. Bashe, J. Thewalt, D. Tieleman, Computational and experimental approaches for investigating nanoparticle-based drug delivery systems, Biochimica et Biophysica Acta (BBA)-Biomembranes, 1858 (2016) 1688-1709.

[132] N. Thota, J. Jiang, Computational amphiphilic materials for drug delivery, Frontiers in Materials, 2 (2015) 64.

[133] A.D. Costache, L. Sheihet, K. Zaveri, D.D. Knight, J. Kohn, Polymer− drug interactions in tyrosine-derived triblock copolymer nanospheres: a computational modeling approach, Molecular Pharmaceutics, 6 (2009) 1620-1627.

[134] X. Guo, L. Zhang, Y. Qian, J. Zhou, Effect of composition on the formation of poly (dl-lactide) microspheres for drug delivery systems: Mesoscale simulations, Chemical Engineering Journal, 131 (2007) 195-201.

[135] X.D. Guo, J.P.K. Tan, L.J. Zhang, M. Khan, S.Q. Liu, Y.Y. Yang, Y. Qian, Phase behavior study of paclitaxel loaded amphiphilic copolymer in two solvents by dissipative particle dynamics simulations, Chemical Physics Letters, 473 (2009) 336-342.

[136] X.D. Guo, J.P. Tan, S.H. Kim, L.J. Zhang, Y. Zhang, J.L. Hedrick, Y.Y. Yang, Y. Qian, Computational studies on self-assembled paclitaxel structures: templates for hierarchical block copolymer assemblies and sustained drug release, Biomaterials, 30 (2009) 6556-6563.

[137] J.P. Tan, S.H. Kim, F. Nederberg, E.A. Appel, R.M. Waymouth, Y. Zhang, J.L. Hedrick, Y.Y. Yang, Hierarchical supermolecular structures for sustained drug release, Small, 5 (2009) 1504-1507.

[138] J. Luo, K. Xiao, Y. Li, J.S. Lee, L. Shi, Y.-H. Tan, L. Xing, R. Holland Cheng, G.-Y. Liu, K.S. Lam, Well-defined, size-tunable, multifunctional micelles for efficient paclitaxel delivery for cancer treatment, Bioconjugate Chemistry, 21 (2010) 1216-1224.

[139] W. Jiang, J. Luo, S. Nangia, Multiscale approach to investigate self-assembly of telodendrimer based nanocarriers for anticancer drug delivery, Langmuir, 31 (2015) 4270-4280.

[140] K. Karatasos, Self-association and complexation of the anti-cancer drug doxorubicin with PEGylated hyperbranched polyesters in an aqueous environment, The Journal of Physical Chemistry B, 117 (2013) 2564-2575.

[141] X. Zeng, Y. Zhang, Z. Wu, P. Lundberg, M. Malkoch, A.M. Nyström, Hyperbranched copolymer micelles as delivery vehicles of doxorubicin in breast cancer cells, Journal of Polymer Science Part A: Polymer Chemistry, 50 (2012) 280-288.

[142] M. Subashini, P.V. Devarajan, G.S. Sonavane, M. Doble, Molecular dynamics simulation of drug uptake by polymer, Journal of Molecular Modeling, 17 (2011) 1141-1147.

[143] X.-Y. Wang, L. Zhang, X.-H. Wei, Q. Wang, Molecular dynamics of paclitaxel encapsulated by salicylic acid-grafted chitosan oligosaccharide aggregates, Biomaterials, 34 (2013) 1843-1851.

[144] P. Shan, J.-W. Shen, D.-H. Xu, L.-Y. Shi, J. Gao, Y.-W. Lan, Q. Wang, X.-H. Wei, Molecular dynamics study on the interaction between doxorubicin and hydrophobically modified chitosan oligosaccharide, RSC Advances, 4 (2014) 23730-23739.

[145] I.F. Tannock, D. Rotin, Acid pH in tumors and its potential for therapeutic exploitation, Cancer Research, 49 (1989) 4373-4384.

[146] X. He, J. Li, S. An, C. Jiang, pH-sensitive drug-delivery systems for tumor targeting, Therapeutic Delivery, 4 (2013) 1499-1510.

[147] E.S. Lee, Z. Gao, Y.H. Bae, Recent progress in tumor pH targeting nanotechnology, Journal of Controlled Release, 132 (2008) 164-170.

[148] J. Liu, Y. Huang, A. Kumar, A. Tan, S. Jin, A. Mozhi, X.-J. Liang, pH-sensitive nano-systems for drug delivery in cancer therapy, Biotechnology Advances, 32 (2014) 693-710.

[149] X.D. Guo, F. Tandiono, N. Wiradharma, D. Khor, C.G. Tan, M. Khan, Y. Qian, Y.-Y. Yang, Cationic micelles self-assembled from cholesterol-conjugated oligopeptides as an efficient gene delivery vector, Biomaterials, 29 (2008) 4838-4846.

[150] X.D. Guo, L.J. Zhang, Z.M. Wu, Y. Qian, Dissipative particle dynamics studies on microstructure of pH-sensitive micelles for sustained drug delivery, Macromolecules, 43 (2010) 7839-7844.

[151] S.Y. Nie, Y. Sun, W.J. Lin, W.S. Wu, X.D. Guo, Y. Qian, L.J. Zhang, Dissipative particle dynamics studies of doxorubicin-loaded micelles assembled from four-arm star triblock polymers 4AS-PCL-b-PDEAEMA-b-PPEGMA and their pH-release mechanism, The Journal of Physical Chemistry B, 117 (2013) 13688-13697.

[152] Y.Q. Yang, B. Zhao, Z.D. Li, W.J. Lin, C.Y. Zhang, X.D. Guo, J.F. Wang, L.J. Zhang, pH-sensitive micelles self-assembled from multi-arm star triblock co-polymers poly (ε-caprolactone)-b-poly (2-(diethylamino) ethyl methacrylate)-b-poly (poly (ethylene glycol) methyl ether methacrylate) for controlled anticancer drug delivery, Acta Biomaterialia, 9 (2013) 7679-7690.

[153] Y.Q. Yang, W.J. Lin, L.J. Zhang, C.Z. Cai, W. Jiang, X.D. Guo, Y. Qian, Synthesis, characterization and pH-responsive self-assembly behavior of amphiphilic multiarm star triblock copolymers based on PCL, PDEAEMA, and PEG, Macromolecular Research, 21 (2013) 1011-1020.

[154] S.Y. Nie, W.J. Lin, N. Yao, X.D. Guo, L.J. Zhang, Drug release from ph-sensitive polymeric micelles with different drug distributions: insight from coarse-grained simulations, ACS Applied Materials & Interfaces, 6 (2014) 17668-17678.

[155] S. Jiang, Z. Cao, Ultralow-fouling, functionalizable, and hydrolyzable zwitterionic materials and their derivatives for biological applications, Advanced Materials, 22 (2010) 920-932.

[156] W. Min, D. Zhao, X. Quan, D. Sun, L. Li, J. Zhou, Computer simulations on the pH-sensitive tri-block copolymer containing zwitterionic sulfobetaine as a novel anti-cancer drug carrier, Colloids and Surfaces B: Biointerfaces, 152 (2017) 260-268.

[157] S. Zhai, Y. Ma, Y. Chen, D. Li, J. Cao, Y. Liu, M. Cai, X. Xie, Y. Chen, X. Luo, Synthesis of an amphiphilic block copolymer containing zwitterionic sulfobetaine as a novel pH-sensitive drug carrier, Polymer Chemistry, 5 (2014) 1285-1297.

[158] J. Liu, L. Cui, D. Losic, Graphene and graphene oxide as new nanocarriers for drug delivery applications, Acta Biomaterialia, 9 (2013) 9243-9257.

[159] M. Mahdavi, F. Rahmani, S. Nouranian, Molecular simulation of pH-dependent diffusion, loading, and release of doxorubicin in graphene and graphene oxide drug delivery systems, Journal of Materials Chemistry B, 4 (2016) 7441-7451.

[160] H. Brem, P. Gabikian, Biodegradable polymer implants to treat brain tumors, Journal of Controlled Release, 74 (2001) 63-67.

[161] R. Ramachandran, V.R. Junnuthula, G.S. Gowd, A. Ashokan, J. Thomas, R. Peethambaran, A. Thomas, A.K.K. Unni, D. Panikar, S.V. Nair, Theranostic 3-Dimensional nano brain-implant for prolonged and localized treatment of recurrent glioma, Scientific Reports, 7 (2017) 43271.

[162] A. Roux, F. Caire, J. Guyotat, P. Menei, P. Metellus, J. Pallud, Carmustine wafer implantation for high-grade gliomas: evidence-based safety efficacy and practical recommendations from the Neuro-oncology Club of the French Society of Neurosurgery, Neurochirurgie, 63 (2017) 433-443.

[163] M. McGinity, J.R. Floyd, J. McGinity, F. Zhang, Implant compositions for the unidirectional delivery of drugs to the brain, Drug Development and Industrial Pharmacy, 43 (2017) 1421-1429.

[164] S.H. Ranganath, Y. Fu, D.Y. Arifin, I. Kee, L. Zheng, H.-S. Lee, P.K.-H. Chow, C.-H. Wang, The use of submicron/nanoscale PLGA implants to deliver paclitaxel with enhanced pharmacokinetics and therapeutic efficacy in intracranial glioblastoma in mice, Biomaterials, 31 (2010) 5199-5207.

[165] H. Dang, J. Wang, J.-X. Cheng, P.-Y. Wang, Y. Wang, L.-F. Cheng, C. Du, X.-J. Wang, Efficacy of local delivery of ardipusilloside I using biodegradable implants against cerebral tumor growth, American Journal of Cancer Research, 5 (2015) 243.

[166] Y. Akiyama, Y. Kimura, R. Enatsu, T. Mikami, M. Wanibuchi, N. Mikuni, Advantages and Disadvantages of Combined Chemotherapy with Carmustine Wafer and Bevacizumab in Patients with Newly Diagnosed Glioblastoma: A Single-Institutional Experience, World Neurosurgery, 113 (2018) e508-e514.

[167] C.-H. Wang, J. Li, C.S. Teo, T. Lee, The delivery of BCNU to brain tumors, Journal of Controlled Release, 61 (1999) 21-41.

[168] W.H.K. Tan, F. Wang, T. Lee, C.H. Wang, Computer simulation of the delivery of etanidazole to brain tumor from PLGA wafers: comparison between linear and double burst release systems, Biotechnology and Bioengineering, 82 (2003) 278-288.

[169] W.H.K. Tan, T. Lee, C.H. Wang, Simulation of intratumoral release of etanidazole: Effects of the size of surgical opening, Journal of Pharmaceutical Sciences, 92 (2003) 773-789.

[170] C.S. Teo, W.H.K. Tan, T. Lee, C.-H. Wang, Transient interstitial fluid flow in brain tumors: Effect on drug delivery, Chemical Engineering Science, 60 (2005) 4803-4821.

[171] A.J. Torres, C. Zhu, M.L. Shuler, S. Pannullo, Paclitaxel delivery to brain tumors from hydrogels: a computational study, Biotechnology Progress, 27 (2011) 1478-1487.

[172] S. Kalyanasundaram, V. Calhoun, K. Leong, A finite element model for predicting the distribution of drugs delivered intracranially to the brain, American Journal of Physiology-Regulatory, Integrative and Comparative Physiology, 273 (1997) R1810-R1821.

[173] T. Nagashima, T. Shirakuni, S.I. Rapoport, A two-dimensional, finite element analysis of vasogenic brain edema, Neurologia Medico-chirurgica, 30 (1990) 1-9.

[174] A.A. Linninger, M.R. Somayaji, M. Mekarski, L. Zhang, Prediction of convection-enhanced drug delivery to the human brain, Journal of Theoretical Biology, 250 (2008) 125-138.

[175] J.H. Kim, G.W. Astary, S. Kantorovich, T.H. Mareci, P.R. Carney, M. Sarntinoranont, Voxelized computational model for convection-enhanced delivery in the rat ventral hippocampus: comparison with in vivo MR experimental studies, Annals of Biomedical Engineering, 40 (2012) 2043-2058.

[176] K.N. Magdoom, G.L. Pishko, L. Rice, C. Pampo, D.W. Siemann, M. Sarntinoranont, MRI-based computational model of heterogeneous tracer transport following local infusion into a mouse hind limb tumor, PloS One, 9 (2014) e89594.

[177] K.M. Tangen, R. Leval, A.I. Mehta, A.A. Linninger, Computational and in vitro experimental investigation of intrathecal drug distribution: parametric study of the effect of injection volume, cerebrospinal fluid pulsatility, and drug uptake, Anesthesia & Analgesia, 124 (2017) 1686-1696.

[178] W. Zhan, D.Y. Arifin, T.K. Lee, C.-H. Wang, Mathematical Modelling of Convection Enhanced Delivery of Carmustine and Paclitaxel for Brain Tumour Therapy, Pharmaceutical Research, 34 (2017) 860-873.

[179] D. Su, R. Ma, L. Zhu, Numerical study of nanofluid infusion in deformable tissues for hyperthermia cancer treatments, Medical & Biological Engineering & Computing, 49 (2011) 1233-1240.

[180] K.H. Støverud, M. Darcis, R. Helmig, S.M. Hassanizadeh, Modeling concentration distribution and deformation during convection-enhanced drug delivery into brain tissue, Transport in Porous Media, 92 (2012) 119-143.

[181] T.P. Butler, F.H. Grantham, P.M. Gullino, Bulk transfer of fluid in the interstitial compartment of mammary tumors, Cancer Research, 35 (1975) 3084-3088.

[182] Y. Boucher, R.K. Jain, Microvascular pressure is the principal driving force for interstitial hypertension in solid tumors: implications for vascular collapse, Cancer Research, 52 (1992) 5110-5114.

[183] S. Raghunathan, D. Evans, J.L. Sparks, Poroviscoelastic modeling of liver biomechanical response in unconfined compression, Annals of Biomedical Engineering, 38 (2010) 1789-1800.

[184] A. Bhandari, A. Bansal, A. Singh, N. Sinha, Perfusion kinetics in human brain tumor with DCE-MRI derived model and CFD analysis, Journal of Biomechanics, 59 (2017) 80-89.

[185] K. Neeves, C. Lo, C. Foley, W. Saltzman, W. Olbricht, Fabrication and characterization of microfluidic probes for convection enhanced drug delivery, Journal of Controlled Release, 111 (2006) 252-262.

[186] S.K. Hobbs, W.L. Monsky, F. Yuan, W.G. Roberts, L. Griffith, V.P. Torchilin, R.K. Jain, Regulation of transport pathways in tumor vessels: role of tumor type and microenvironment, Proceedings of the National Academy of Sciences of the United States of America, 95 (1998) 4607-4612.

[187] F. Yuan, M. Leunig, S.K. Huang, D.A. Berk, D. Papahadjopoulos, R.K. Jain, Microvascular permeability and interstitial penetration of sterically stabilized (stealth) liposomes in a human tumor xenograft, Cancer Research, 54 (1994) 3352-3356.

[188] F. Yuan, H.A. Salehi, Y. Boucher, U.S. Vasthare, R.F. Tuma, R.K. Jain, Vascular permeability and microcirculation of gliomas and mammary carcinomas transplanted in rat and mouse cranial windows, Cancer Research, 54 (1994) 4564-4568.

[189] C. Lei, Y. Cui, L. Zheng, P.K.-H. Chow, C.-H. Wang, Development of a gene/drug dual delivery system for brain tumor therapy: potent inhibition via RNA interference and synergistic effects, Biomaterials, 34 (2013) 7483-7494.

[190] Y.L. Jiang, Y. Zhu, A.B. Moore, K. Miller, A.-M. Broome, A Biotinylated Bioluminescent Probe for Long Lasting Targeted In Vivo Imaging of Xenografted Brain Tumors in Mice, ACS Chemical Neuroscience, 9 (2018) 100-106.

[191] P.K. Kreeger, D.A. Lauffenburger, Cancer systems biology: a network modeling perspective, Carcinogenesis, 31 (2009) 2-8.

[192] J.H. Sampson, R. Raghavan, M.L. Brady, J.M. Provenzale, J.E. Herndon, D. Croteau, A.H. Friedman, D.A. Reardon, R.E. Coleman, T. Wong, Clinical utility of a patient-specific algorithm for simulating intracerebral drug infusions, Neuro-oncology, 9 (2007) 343-353.

[193] R. Raghavan, M.L. Brady, J.H. Sampson, Delivering therapy to target: improving the odds for successful drug development, Therapeutic Delivery, 7 (2016) 457-481.

Appendix

PBPK model for nanoparticle-mediated drug delivery

Compartment	Nanoparticle encapsulated drugs (NP)	Free drugs (FD)	Bound Drug (BD)
NT	$V_{NP,NT}\frac{dC_{NP,NT}}{dt} = k_{NP,BP-NT}V_{NP,BP}C_{NP,BP}$ $-k_{NP,NT-BP}V_{NP,NT}C_{NP,NT}$ $-k_{rel,NT}V_{NP,NT}C_{NP,NT}$	$V_{FD,NT}\frac{dC_{FD,NT}}{dt} = k_{FD,BP-NT}V_{FD,BP}C_{FD,BP}$ $-k_{FD,NT-BP}V_{FD,NT}C_{FD,NT} + k_{ds,NT}V_{BD,NT}C_{BD,NT}$ $-k_{as,NT}V_{FD,NT}C_{FD,NT} + k_{rel,NT}V_{NP,NT}C_{NP,NT}$	$V_{BD,NT}\frac{dC_{BD,NT}}{dt} = k_{BD,BP-NT}V_{BD,BP}C_{BD,BP}$ $-k_{BD,NT-BP}V_{BD,NT}C_{BD,NT} + k_{as,NT}V_{FD,NT}C_{FD,NT}$ $-k_{ds,NT}V_{BD,NT}C_{BD,NT}$
BP	$V_{NP,BP}\frac{dC_{NP,BP}}{dt} = Q(C_{NP,IVS} - C_{NP,BP})$ $-(k_{NP,BP-NT} + k_{rel,BP})V_{NP,BP}C_{NP,BP}$ $+k_{NP,NT-BP}V_{NP,NT}C_{NP,NT}$ $-k_{cl,NP}V_{NP,BP}C_{NP,BP}$	$V_{FD,BP}\frac{dC_{FD,BP}}{dt} = k_{rel,BP}V_{NP,BP}C_{NP,BP}$ $+k_{FD,NT-BP}V_{FD,NT}C_{FD,NT} - k_{FD,BP-NT}V_{FD,BP}C_{FD,BP}$ $-Q(C_{FD,BP} - C_{FD,IVS}) + k_{ds,BP}V_{DB,BP}C_{DB,BP}$ $-k_{as}V_{FD,BP}C_{FD,BP} - k_{cl,FD}V_{FD,BP}C_{FD,BP}$	$V_{BD,BP}\frac{dC_{BD,BP}}{dt} = k_{BD,NT-BP}V_{BD,NT}C_{BD,NT}$ $-k_{BD,BP-NT}V_{BD,BP}C_{BD,BP} + Q(C_{BD,IVS} - C_{BD,BP})$ $+k_{as,BP}V_{FD,BP}C_{FD,BP} - k_{ds,BP}V_{BD,BP}C_{BD,BP}$ $-k_{cl,BD}V_{BD,BP}C_{BD,BP}$
IVS	$V_{NP,IVS}\frac{dC_{NP,IVS}}{dt} = Q(C_{NP,BP} - C_{NP,IVS})$ $-(k_{NP,IVS-ECS} + k_{rel,IVS})V_{NP,IVS}C_{NP,IVS}$ $+k_{NP,ECS-IVS}V_{NP,ECS}C_{NP,ECS}$	$V_{FD,IVS}\frac{dC_{FD,IVS}}{dt} = Q(C_{FD,BP} - C_{FD,IVS})$ $+k_{FD,ECS-IVS}V_{FD,ECS}C_{FD,ECS} + k_{rel,IVS}V_{NP,IVS}C_{NP,IVS}$ $-k_{FD,IVS-ECS}V_{FD,IVS}C_{FD,IVS} + k_{ds,IVS}V_{BD,IVS}C_{BD,IVS}$ $-k_{as,IVS}V_{FD,IVS}C_{FD,IVS}$	$V_{BD,IVS}\frac{dC_{BD,IVS}}{dt} = k_{BD,ECS-IVS}V_{BD,ECS}C_{BD,ECS}$ $-k_{BD,IVS-ECS}V_{BD,IVS}C_{BD,ECS} + Q(C_{BD,BP} - C_{BD,IVS})$ $+k_{as,IVS}V_{FD,IVS}C_{FD,IVS} - k_{ds,IVS}V_{BD,IVS}C_{BD,IVS}$
ECS	$V_{NP,ECS}\frac{dC_{NP,ECS}}{dt} =$ $k_{NP,IVS-ECS}V_{NP,IVS}C_{NP,IVS}$ $-k_{rel,ECS}V_{NP,ECS}C_{NP,ECS}$ $-k_{NP,ECS-IVS}V_{NP,ECS}C_{NP,ECS}$	$V_{FD,ECS}\frac{dC_{FD,ECS}}{dt} = k_{FD,IVS-ECS}V_{FD,IVS}C_{FD,IVS}$ $-k_{FD,ECS-IVS}V_{FD,ECS}C_{FD,ECS} + k_{rel,ECS}V_{NP,ECS}C_{NP,ECS}$ $+k_{FD,ICS-ECS}V_{FD,ICS}C_{FD,ICS} + k_{ds,ECS}V_{BD,ECS}C_{BD,ECS}$ $-k_{FD,ECS-ICS}V_{FD,ECS}C_{FD,ECS} - k_{as,ECS}V_{FD,ECS}C_{FD,ECS}$	$V_{BD,ECS}\frac{dC_{BD,ECS}}{dt} = k_{BD,IVS-ECS}V_{BD,IVS}C_{BD,IVS}$ $-k_{BD,ECS-IVS}V_{BD,ECS}C_{BD,ECS} + k_{as,ECS}V_{FD,ECS}C_{FD,ECS}$ $-k_{ds,ECS}V_{BD,ECS}C_{BD,ECS}$
ICS	N.A .	$V_{FD,ICS}\frac{dC_{FD,ICS}}{dt} = k_{FD,ECS-ICS}V_{FD,ECS}C_{FD,ECS}$ $-k_{FD,ICS-ECS}V_{FD,ICS}C_{FD,ICS} + k_{ds,ICS}V_{BD,ICS}C_{BD,ICS}$ $-k_{as,ICS}V_{FD,ICS}C_{FD,ICS}$	$V_{BD,ICS}\frac{dC_{BD,ICS}}{dt} = k_{as,ICS}V_{FD,ICS}C_{FD,ICS}$ $-k_{ds,ICS}V_{BD,ICS}C_{BD,ICS}$

as - Drug associating with proteins; *cl* - Drug clearance; *ds* - Drug disassociating with proteins; *k* - rate for transport or reaction; *rel* - Drug release from nanoparticles